Effects of Pre-Salt Relief on Salt Tectonics on the São Paulo Plateau and Implications for the Albian Gap

*Leonardo M. Pichel[1], Christopher A-L. Jackson[2,3]; Frank Peel[3,2], Tim P. Dooley[3]

1 – School of Earth and Environmental Sciences, University of Manchester, Oxford Road, Manchester M13 9PL, UK

2 – Basins Research Group (BRG), Department of Earth Science and Engineering, Imperial College London, South Kensington Campus, SW7 2BP, United Kingdom

3 – The University of Texas at Austin, Bureau of Economic Geology, Jackson School of Geosciences, Austin, Texas, USA

Key-words: SALT TECTONICS, MINIBASINS, DIAPIRISM, TRANSLATION, BASE-SALT RELIEF, RAMP-SYNCLINE BASINS, GRAVITY-DRIVEN DEFORMATION, SANTOS BASIN

ABSTRACT

Pre-salt relief has been recently shown to significantly influence salt flow, producing three-dimensionally complex strain distribution and multiphase deformation within the evaporite sequence and overburden. The São Paulo Plateau, Santos Basin, Brazil is a prolific hydrocarbon province situated downdip of the Albian Gap, characterized by > 2 km thick, mechanically layered Aptian salt, prominent basal relief and a complex framework of supra-salt structures. This study uses 3D seismic data combined with physical and kinematic models to demonstrate how gravity-driven translation above thick salt with complex basal relief generated this framework. A series of ramp-syncline basins occur above and downdip of the main pre-salt highs indicating c. 30 km of translation in the area. As the system translated downdip, salt flux variations caused by significant base-salt relief resulted in non-uniform motion of the cover with simultaneous development of extensional and contractional structures and multiphase reactivation during the Late Cretaceous-Paleocene. Contraction occurred preferentially above landward-dipping ramps at base of salt and downdip of basinward-dipping ramps where motion decelerated. Extension occurred at the top of basinward-dipping ramps and base-salt plateaus, where flow accelerated. Where base-salt was broadly flat, structures evolved primarily by density-driven subsidence and diapirism. At the edge of or around smaller base-salt highs, salt structures were affected by plan-view rotation, shearing and radial flow. To the north, where earlier Albian growth occurred, deformation is marked by a polygonal plan-view framework that is also a consequence of oblique flow driven by the concave shape of the margin. These observations contribute to the long-lived debate regarding the mechanisms of salt tectonics in the SPP and the

equally controversial Albian Gap, ultimately improving the general understanding of the effects of base-salt relief and regionally complex salt tectonics.

1. Introduction

Gravity-driven salt-related deformation in passive margins is understood as dynamic domains of updip extension and downdip contraction kinematically connected by an intermediate, broadly undeformed zone of translation (Fig. 1a) (Rowan et al., 2000; 2004; Hudec and Jackson, 2004, 2007; Brun and Fort, 2011; Quirk et al., 2012; Jackson et al., 2015a). Recent studies (Dooley et al., 2017; Dooley and Hudec, 2017; Pichel et al., 2018a,b), demonstrated this represents a simplified view of salt tectonics as salt is sensitive to the surface it flows across, so salt-detached translation over pre-salt topography results in complex, multiphase deformation and strain distribution (Fig. 1b). Thus, translational domains, previously thought as simpler, low-strained salt provinces, can undergo highly complex structural histories. This understanding can improve the analysis of regional salt tectonics along various continental margins and contribute to long-lived debates, such as the origin of the Albian Gap and evolution of the São Paulo Plateau (SPP), Santos Basin, Brazil (Davison et al., 2012; Fiduk and Rowan, 2012; Jackson et al., 2015b).

The area focus of this paper, the São Paulo Plateau (SPP, Fig. 1c), is characterized by an intricate pattern of salt diapirs and minibasins formed above a thick, layered, salt sequence (> 2 km, Davison et al., 2012, Fiduk and Rowan 2012; Jackson et al., 2015b). The area is located at the present-day toe-of-slope at an intermediate position downdip of the enigmatic Albian Gap and updip of a c. 30 km wide salt nappe at the downdip end of the basin (Davison et al., 2012; Quirk et al., 2012; Jackson et al., 2015b) (Fig. 1c-d). The SPP is also situated above series of base-salt

steps or highs (Fig. 1d and 2) (Davison et al., 2012; Alvez et al., 2017), some of which are associated with the largest hydrocarbon discoveries in the last decades (Mohriak et al., 2012). At least four (Gamboa et al, 2008; Rodriguez et al., 2018) or six (Fiduk and Rowan 2012) units are recognized within the salt interval due to differences in composition and seismic facies. Halite-rich units (>85%, A1 and A3, Rodriguez et al., 2018) are characterized by transparent and chaotic seismic facies, whereas units with higher proportion of anhydrites and bittern salts (15-35%, A2 and A4) present highly reflective seismic facies (Rodriguez et al., 2018, their figures 4 and 5).

The evolution, kinematics and unique structural style of the SPP and its neighbouring Albian Gap have been subject of intense controversy in the last decades. Some authors suggest Albian and Late Cretaceous deformation was driven by regional shortening of the supra-salt cover over the entire SPP in response to contemporaneous updip extension (e.g. Quirk et al 2012; Fiduk and Rowan 2012; Guerra and Underhill, 2012; Alves et al 2016). Fiduk and Rowan (2012), for example, attribute higher contractional strains within the salt sequence relative to the cover due to basinward flow and strain partionining across intra-salt detachments. Guerra and Underhill (2012) suggests salt flow occurred in multiple directions due to a switch of sediment supply in the Eocene resulting in a polygonal pattern of salt structures in the area; whereas Cobbold et al. (1995) suggest this was a consequence of convergent gliding due to the concave shape of the margin (Fig. 1c). Alves et al. (2017) argue ridge push and basinward flow driven by viscous salt drag resulted in eastward increasing contraction and tectonic erosion of strongly lithified pre-salt carbonates.

Other authors, although recognize shortening as a dominant process in the area suggest no major translation occurred (e.g. Rodriguez et al., 2018). In addition to the debate regarding the origin and kinematics of shortening, other authors suggest that the main, Late Cretaceous phase of deformation in the SPP was not driven by regional shortening (Ge et al., 1997; Jackson et al., 2015b; Dooley et al 2015; Jackson and Hudec, 2017). These authors argue that after an initial phase of Albian shortening, Late Cretaceous deformation was dominated by density-driven salt inflation with localized shortening and extension due to large-scale salt expulsion and welding below the updip Albian Gap.

Models of Late Cretaceous regional shortening in the SPP invoke coeval updip extension accommodated by a large landward-dipping listric fault, the Cabo Frio Fault (CFF) and the associated 50-60 km wide Albian Gap (Fig. 1c-d) (Quirk et al., 2012; Fiduk and Rowan 2012; Guerra and Underhill, 2012). Conversely, models invoking a dominant inflation-driven evolution of the SPP relate it to coeval updip expulsion and no Late Cretaceous extension in the Albian Gap, although extension occurred during the Albian generating a c. 60 km wide salt wall that was later expelled seaward (Jackson et al., 2015a; Jackson and Hudec, 2017). The evolution of the Albian Gap and SPP are, thus, intrinsically connected, so understanding the kinematics of one of them can contribute significantly towards the other.

A recent study describes the geometries and 3D kinematics of salt-related asymmetric depocentres recording 28-32 (+2) km of Late Cretaceous-Paleocene basinward translation over base-salt relief in the SPP (Pichel et al., 2018). This type of asymmetric minibasin was first recognized in the Kwanza and Lower Congo Basins, Angola (Marton et al., 1998; Peel et al., 1998; Jackson et al., 2001; Jackson and Hudec, 2005) as formed by translation over base-salt ramps and thus, being

defined as ramp-syncline basins (RSBs). Although Pichel et al. (2018) demonstrates evidence of significant downdip translation and associated salt flux variations over pre-salt relief on minibasins on the SPP; they do not detail how these processes control three-dimensionally complex salt deformation through time or the regional implications for the Central Santos Basin.

Understanding what drives and controls deformation on the SPP is important not only academically but also for the ongoing hydrocarbon exploration in the margin, as this has important implications on the timing of deformation relative to deposition of petroleum systems key elements (Jackson et al., 2015a; Allen et al., 2016). Additionally, the comprehension of the kinematics and, thus, dynamics of salt-driven deformation allows confident evaluation of distribution of stress-strain through time, location and timing of salt-related structural traps, reducing difficulties and uncertainties in balancing regional cross-sections (Allen et al., 2016).

In this study, we analyse the development of the different salt-related structural styles on the SPP, in order to explain the multiphase history, as well as the distribution through time and space of salt structures and minibasins. Our goal is to answer the following questions: 1) what are the main structural processes controlling salt tectonics on the SPP?; 2) How does translation of salt and overburden across pre-salt structures influence the styles of diapirism and minibasins?, and; 3) what are the regional implications of this study and can it shed light on the origin of the enigmatic Albian Gap?

2. Tectono-Stratigraphic Framework

The São Paulo Plateau (SPP) is an area of thick Aptian salt with marked intra-salt mechanical layering and a complex pattern of salt diapirs and anticlines (Fig. 2)

(Davison et al., 2012; Guerra and Underhill, 2012; Fiduk and Rowan, 2012; Mohriak et al., 2012; Jackson et al., 2014a,b; 2015b). The pre-salt interval is characterized by NE-oriented grabens and half-grabens formed during late Barremian-early Aptian rifting. These basins are filled by non-marine clastic strata and overlain by shallow-marine carbonates (Meisling et al., 2001; Modica and Brush, 2004; Karner and Gambôa, 2007; Mohriak et al., 2008, 2009; Contreras et al., 2010). During the late Aptian, fault activity was reduced and a 2.4–2.6 km thick post-rift salt succession was deposited (Fig. 2) (Davison et al., 2012). Although deposition was post-rift, the inherited syn-rift topography impacted salt deposition in the SPP and on the most distal portions of the Santos Basin. This is evidenced by the presence of prominent base-salt highs and ramps associated with monoclinal drape of syn-rift strata and/or minor faulting (Fig. 2) (Davison et al., 2012; Alves et al., 2017; Rodriguez et al., 2018; Pichel et al., 2018).

During the early Albian, the Santos Basin experienced fully marine conditions due to thermally-induced subsidence and eustatic rise. This resulted in widespread deposition of carbonate-dominated succession that is up to c. 1 km thick landward and thins to c. 200-300 m basinward in the study-area (Fig. 1d and 2), where it is characterized by fine-grained marl-dominated strata (Modica and Brush, 2004). During the late Albian, thermal and isostatic subsidence tilted the basin south-eastward, inducing gravity gliding. This produced an array of thin-skinned, predominantly seaward-dipping salt-detached normal faults that dismembered the Albian carbonate platform into extensional rafts updip of the study-area (Demercian et al., 1993; Cobbold et al., 1995; Mohriak et al., 1995; Guerra and Underhill, 2012; Quirk et al., 2012). Throughout the Late Cretaceous to Paleocene sedimentation was dominated by siliciclastic progradation and turbidite deposition due to landward uplift

of the Serra do Mar mountain range (Modica and Brush, 2004). By the end of the Paleocene, sea-level fall resulted in the development of a major regional unconformity, leading to erosion of shelf and slope sediments, and causing their deposition further basinward. Inflated salt on the SPP acted as a topographic barrier to basinward transportation of coarse clastics from the end of the Paleocene onward (Modica and Brush, 2004), resulting in widespread mud deposition.

3. Methods

This study uses a zero-phase processed, time-migrated, 3D seismic reflection dataset that covers 20,122 km^2 of the SPP, Central Santos Basin, Brazil (Fig. 1c). Inline (west-east) and crossline (north-south) spacing is 18.75 and 25 m, respectively. Vertical sampling interval is 4 ms two-way time travel (ms TWT) and total record length is of 5500 ms TWT. The survey display follows the Society of Economic Geologists normal polarity, where a downward increase in acoustic impedance is represented by a positive reflection event (white on seismic sections) and a decrease in acoustic impedance by a negative event (black on seismic section) (Brown, 2011). The average dominant frequency in the Aptian salt is c. 36 Hz and the interval velocity is c. 4400 m/s, yielding a vertical resolution of c. 29 m (Rodriguez et al., 2018). The relatively lower velocity of the salt is due to the intra-salt lithological heterogeneity and, more specifically, the presence of acoustically slower potash intervals (Jackson et al., 2015b). Overburden strata have a dominant frequency that varies with depth from c. 40-31 Hz and a slower average interval velocity (c. 1900-2015 m/s), which together result in higher vertical resolution (c. 12-17 m) that decreases with depth (Jackson et al., 2015b; Rodriguez et al., 2018). Horizontal resolution is twice the seismic line spacing (i.e., 37.5 m in the E–W direction and 50 m in the N–S direction) (Jackson et al 2015). We also use three

PSDM seismic transects, c. 350 km long, broadly parallel to the tectonic transport direction (i.e. NW-SE), which are fundamental to investigate the timing and styles of salt-related deformation in the SPP in a regional context, their relationship with base-salt topography, and the Albian Gap (Fig. 2).

In order to analyse the 3D evolution of salt structures and minibasins with variable orientation, we conduct 3D seismic mapping using the same approach described in in Pichel et al., 2018. Identification of key seismic stratigraphic surfaces, such as the base and top salt, top Albian (TA), top-Cretaceous (TC), early- and late Paleocene unconformity (EP and LP) and top Paleocene (TP) was based on age and well-control of previous publications (Guerra and Underhill, 2012; Jackson et al., 2015b; Rodriguez et al., 2018). A base-salt static-corrected map (Fig. 3) was used in order to understand the orientation, structural relief and relationship of pre-salt topography with salt and supra-salt stratigraphic-architecture. The resulting map is in TWT, not depth, and it represents where the image would be if the salt were replaced by an equivalent thickness of sediment (Pichel et al., 2018a). Although the map present small-scale high-frequency artefacts (NW edge), it is notably similar to published depth-maps using PSDM 3D data (Alves et al., 2017) and to the base-salt structure imaged in the 2D PSDM sections (Fig. 2). This attests the efficiency of the method and the suitability of the map for interpretation of large base-salt structures (Pichel et al., 2018a).

4. Pre-salt structures

The SPP is defined by two large pre-salt highs: the NNE-oriented Sugar-Loaf Sub-High in the south; and the NE-oriented Tupi Sub-High to the north (Mohriak et al., 2012, Rodriguez et al., 2018). These highs are connected by an ENE relay zone

(Fig. 3) and are part of a larger structure denominated as the Outer High, which is characterized predominantly by half-grabens formed during rifting (Fig. 3) (Demercian, 1996; Davison et al., 2012). The highs are bound by sets of large NNE-NE trending normal faults with cumulative throw from 0.4-0.8 s (c. 0.9-1.8 km) with syn-rift hangingwall growth strata, and are oriented roughly perpendicular to the main direction of gravity-driven transport in the basin, i.e. ESE to SE (Davison et al., 2012; Quirk et al., 2012). The base of salt is largely concordant with pre-salt units (Fig. 2), but a small number of faults offset the base of salt by up to 100 ms TWT (c. 450 m) forming monoclinal geometries at the base-salt over the largest pre-salt highs (Davison et al., 2012; Alves et al., 2017; Rodriguez et al 2017). This evidence indicates that pre-salt structures and related topography were present before and during salt deposition, with only minor, reduced fault activity during salt deposition (Davison et al., 2012). This resulted in non-uniform salt deposition with thicker (> 2 km), halite-richer and, thus, more mobile salt over pre-salt lows and thinner (c. 1 km) salt over highs (Davison et al., 2012; Rodriguez et al., 2018).

The Tupi high is on average 20 km wide has a maximum structural relief of 0.9 s (1.5-2 km) being limited by a steep basinward-dipping SE edge defined by series of basinward-dipping faults; and a gentle to sub-horizontal, less faulted NW flank. Its northern margin is defined by a steep NW-oriented edge, where the Tupi High branches to a narrower, 10 km wide, NNW-oriented horst (H2 of Alves et al., 2017, fig. 3c) (Fig. 3). Two smaller base-salt steps with similar trend and geometry to the Tupi appear 10 and 15 km downdip and another 4km to the NE, being defined by narrow tilted fault-blocks with structural relief of 04-0.6 s (c.0.9-1.2 km) (Fig. 3). A broader, semi-rectangular high (H4 of Alves et al., 2017, fig. 3c) appears 10 km downdip from the centre of the Tupi High at the edge of the data (Fig. 3).

The Sugar Loaf High is broader than the Tupi High with a 45-50 km wide plateau and a steep updip margin defined by series of landward-dipping faults, which produce two significant landward-dipping base-salt ramps with 0.5 s (c. 1 km) of relief (Fig 3). Its downdip edge is characterized by basinward-dipping faults defining a single basinward-dipping base-salt ramp with c. 1 km of relief (Fig. 3). The Sugar Loaf High presents more structural complexity than the Tupi as it broadens southwards, its edges curve along-strike from NNE in the south to NE in the north; and smaller NE horsts branch out from its northern edge (Fig. 3).

5. Salt and Overburden structures

The area comprises a complex framework of salt diapirs and anticlines with variable orientation and evolution (Fig. 4) (Davison et al., 2012; Guerra and Underhill, 2012; Quirk et al., 2012; Jackson et al., 2015b). Diapirs consist mainly of salt walls with curvilinear planform (Fig. 4). Salt structures and minibasins are predominantly sub-parallel to pre-salt structure in their vicinity in the south and central portions of the study-area, whereas a more polygonal pattern of structures is observed towards the north-northeast (Figs. 3-4) (Guerra and Underhill, 2012; Jackson et al., 2015b).

In order to explain the distribution of different structural styles, we divide the area into six domains according to salt and overburden geometries, tectono-stratigraphic evolution and relationship with base-salt structures (Figs 3-4). These domains expand on recent divisions that were based primarily on the relationship between salt thicknesses, composition and base salt topography (Rodriguez et al., 2018), focusing on the kinematics and geometries of salt walls and minibasins (Figs. 3-4).

5.1. Domain I: West of Sugar Loaf

Description

Domain I is located west of the Sugar Loaf High above its gentle landward-dipping edge and is characterized by a NE-oriented salt-cored fold belt, along with curvilinear salt walls and minibasins with variable orientations (Figs. 2, 3 and 4). Salt-cored folds trend mainly NE, curving gently northwards to a NNE trend, sub-parallel to the updip edge of the Sugar Loaf High (Figs. 3-4). The folds are 4-15 km long, 1-3 km wide and with 3-5 km of wavelength (Figs. 4-5). They have angular to box-fold profiles, and are predominantly upright with little or no preferred vergence (Fig. 5a-c). The folds are commonly cored by intra-salt seaward-vergent sear zones and affected by pairs of inward-dipping normal faults without any syn-depositional growth and, thus, associated with outer-arc extension (Fig. 5a-c); indicating they are driven by lateral shortening. In a few cases, minor reactive diapirism associated with normal faults at the crests of some folds suggests reactivation by weak, late-stage extension, which typically occurs over base-salt flats further basinward (Fig. 5a-c). These folds become dormant upward in the Paleocene, with the easternmost (i.e. seaward) ones being defined by a tabular, c. 250m thick, pre-kinematic Albian roof onlapped by Upper Cretaceous to early Paleocene growth strata. To the west, the tabular pre-kinematic section (sub-vertical white lines) becomes broadly thicker and younger landward, being also composed of post-Albian strata (Figs. 5a-c).

Highly-curved and tall (up to 4.9 km) salt walls with variable orientation, mostly N-NNW (Fig. 5d), nucleate from salt anticlines in the south (Fig. 4, easternmost walls of figs. 5a-b), presenting a wider range of geometries than other walls in the SPP. They have a broadly isopachous Albian interval that can be upturned (Fig. 5b) and offset by inward-dipping and younging normal faults exhibiting growth during the Late Cretaceous (Fig. 5a-b and d). These geometries are similar to the adjacent salt-

cored folds, suggesting the walls were initiated by the same process, i.e. Late Cretaceous shortening, and were later reactivated by reactive diapirism during Late Cretaceous/early Paleocene (Fig. 5a-b and d). In some cases, the walls uplift a c. 800 m thick, extensionally thinned Paleocene roof (Fig. 5b), suggesting Neogene active diapirism.

Depocentres are also curvilinear, trending mainly NE (Fig. 4) and being predominantly characterized by relatively symmetric, thin (c. 200-500 m) and narrow (1-4 km wide) growth synclines that form by shortening between salt anticlines and above thick salt (c. 2km on average, Rodriguez et al., 2018) (Fig. 5a). The largest and thickest minibasins occur at the northern edge of the area over present-day thinner salt (> 1 km, fig. 5d) with a more variable orientation (NNE-NW, fig. 4).

They are relatively symmetric in cross-section, becoming gradually thicker towards their centre where top-salt and, occasionally, top-Albian lie below the data-set, suggesting drastically thinned salt due to expulsion beneath the subsiding minibasin (Fig. 5d). Thinning and onlapping of latest Cretaceous/Paleocene strata onto an upturned Albian/Upper Cretaceous carapace that is extended by inward-dipping growth faults indicates these walls rose by extension in the latest Cretaceous, although minor Albian-Late Cretaceous growth also occurred (Fig. 5d). The main growth, however, is ongoing and still vigorous, being driven by post-Paleocene density-driven subsidence and salt expulsion due to ponding of thick MTCs (400-600 m each) and, secondarily, by extension (Fig. 5d).

Interpretation

The most prominent structural element in the area is a landward-younging fold-belt sub-parallel to a landward-dipping base-salt ramp defining the landward edge of the

Sugar Loaf High, with sporadic salt walls nucleating from the core of salt anticlines (Fig. 5). Intra-salt shear zones in the core of the salt-cored anticlines suggest movement occurred with a strong component of viscous shear drag within the salt (i.e. Couette flow) and that deformation was mainly driven by lateral shortening. Shortening occurred as flow was buttressed against the Sugar Loaf High promoting salt inflation and overburden contraction, as simulated in recent physical and numerical modelling studies (Dooley et al., 2017; Pichel et al., 2018a,b). Extension and development of reactive diapirism in the core of some of these anticlines appears to be associated with areas where the base-salt flattens and allows flow to accelerate, a feature also seen in recent modelling work (Dooley et al., 2017; Pichel et al., 2018b). The fold belt is part of a large translation system, as identified in Pichel et al. (2018), whose evolution is strongly linked with Domain II further downdip.

5.2. Domain II: Sugar Loaf

Description

The Sugar Loaf, a domain defined by a broad and complex NNE-oriented pre-salt horst (i.e. Sugar Loaf High), is dominated by long (35-50 km) and wide (6-12 km) salt walls (Figs. 3-4). A few NE-trending anticlines also occur at the SW boundary near Domain I, above base-salt landward-dipping ramps at the updip edge of the Sugar Loaf High (Figs. 3-4). Salt-cored folds have similar characteristics to the ones in Domain I (section 5.1, figs. 5 and 6). Salt walls have a dominant N-NNE trend, parallel to the Sugar Loaf High, whereas the ones further downdip become NE-oriented (Figs. 3-4), sub-parallel to the near ENE-NE relay zone downdip.

The salt walls in Domain II are highly complex in cross-section, being characterized by: a) direct onlap, thinning and intense upturn of Albian strata, usually near their centre where they are wider (e.g. wall 3, fig. 6a), or; b) by sub-horizontal to moderately upturned tabular Albian extensionally thinned by inward-dipping growth faults during Late Cretaceous/early Paleocene (Fig. 6b-c). In both cases, Albian-Upper Cretaceous strata are completely separated by diapirs and the Upper Cretaceous/early Paleocene growth interval is highly asymmetric and characterized by dominantly landward-thickening and younging strata typical of ramp-syncline basins (RSBs, fig. 6a-c) (Jackson and Hudec, 2005; Pichel et al., 2018). Such basins form by basinward translation over base-salt ramps, onlapping an Albian/Cenomanian section on the walls eastern flanks whilst being truncated by a top unconformity on the western flank of a basinward salt wall (Fig. 6). Upper RSB strata also appear in direct contact with salt walls whilst being extended by inward-dipping growth faults of same age (RSB 2a-b, fig. 6a-c). Extensional growth is evidenced by the gentle inward-dip and thickening of equivalent strata towards the diapir (eastern flank of walls 1-2, fig. 6a and 2-3 in fig. 6b-c; and triangular diapirs of figs 6d-e). These geometries indicate a local, earlier phase of active rise during early Albian for the largest walls, followed by partial burial at the end of Albian and renewed growth during the Late Cretaceous-Paleocene.

Diapir shapes vary from triangular at their low-relief ends, where growth starts later (early to mid-Late Cretaceous, fig. 6c), to wider, taller and roughly flat-topped walls with stronger flank upturn and complex intra-salt deformation towards their centre (Fig. 6). At their low-relief edges narrow triangular diapirs nucleate over broader and rounder salt structures composed of a mildly upturned Albian-Upper Cretaceous section offset by inward-dipping normal faults at their flanks (Fig. 6d-e). These

diapirs are surrounded by gentle anticlines of same age, indicating the diapirs were formed by reactive piercement at the core of earlier anticlines whose roof was previously uplifted and thinned by erosion and/or outer-arc extension as in Domain I (Figs. 5 and 6d-e). Latest Cretaceous/early Paleocene anticlines also appear within RSBs (Pichel et al., 2018), folding them during their later stages (intra-RSB 2a anticline, fig. 6a).

Interpretation

As walls started growing later (Late Cretaceous onwards) at their edges, these younger portions present a simpler evolution that can be used as a guide to understand the more complex and sometimes incomplete tectono-stratigraphic record in their centre. There, intra-salt reverse shear zones occasionally associated with feeders of intra-salt sheets and overturned flaps, coupled with adjacent, parallel salt-cored folds indicate the walls were affected by at least one phase of shortening (Jackson et al., 2015b). Intra-salt shortening, however, cannot account for all the complex intra-salt deformation (Jackson et al., 2015b; Dooley et al., 2015) and, especially supra-salt extensional geometries, nor provide constraints in the timing of shortening (Cartwright et al., 2012; Fiduk and Rowan, 2012; Jackson et al., 2015b).

Dismembering and greater upturn of the Albian section relative to the onlapping Upper Cretaceous/Paleocene RSBs suggest shortening occurred immediately post-Albian, resulting in an initial phase of active rise, and eventually passive rise as the walls reached the sea-floor at their centre (walls 2-4, fig. 6a-c). The presence of inward-dipping growth normal faults associated with triangular reactive diapirs at the low-relief ends of these walls suggest that active rise was followed by Late Cretaceous-Paleocene extension (Fig. 6d-e). Progressive faulting and reactive rise

may have resulted in further roof thinning, active piercement and eventually passive growth as the diapir reached the seafloor (walls 2-4, fig. 6a-c) at their centre. Where salt walls had reached the sea-floor (i.e. passive diapir), extension was cryptic due to the lack of a roof to record extension (see Jackson and Hudec, 2017), and accommodated mostly by diapir widening, which explains their larger width, generally, where they started growing during Albian/Cenomanian (Walls 2-4, figs 4 and 6a-b). Late intra-RSB folding occurred due to pinning and localized contraction against base-salt steps and, secondarily, by density-driven subsidence (Fig. 6a). Thickness changes, faulting and folding were dramatically reduced at the end of translation during the Paleocene implying that salt movement was minor and mainly related to extensional fall and additional widening (Walls 2-4, fig. 6), but also active rise (Wall 1, fig. 6a).

This multistage diapirism in Domains II and the fold-belt of Domain I are consistent with physical (Dooley et al., 2017, 2018) and numerical models (Pichel et al., 2018a, b) of translation over base-salt landward-dipping ramps. A kinematic model combining the advances of both modelling approaches and based on seismic examples from the study-area is presented here to illustrate the structural evolution of these two domains (Fig. 7). As salt moves from an area of thick salt updip to thin salt over the base-salt high, the flux mismatch results in inflation against landward edge of the ramp and development of a RSB basinward (Fig. 7a-b, phases I-II). An earlier thinned roof (phase I) allows salt to rise as an active diapir (Fig. 7a), whereas an earlier tabular roof results in less salt rise and development of buckle-folds with outer-arc extension (Fig. 7b). The system becomes partially pinned over the ramp resulting in asymmetric growth, i.e. increased inflation and uplift on the landward side, and extension and/or widening of the basinward side over the base-salt plateau

(Figs. 6a-c and 7, phase III). This occurs because as salt gradually thickens, basal-drag is reduced and salt accelerates, reversing strain-patterns after an initial phase of inflation over the base-salt flat (Dooley et al., 2017; 2018). This increase of velocity and salt thickening eventually causes the system to leave the ramp, moving over the base-salt plateau whilst a new anticline develops over the ramp and a new RSB over the high (Fig. 7a-b, phase IV). In the case of an earlier active diapir, continuous inflation allows the diapir to reach the surface, so extension is cryptic and accommodated by diapir widening (Fig. 7a), which explains the > 10 km wide walls over the Sugar-Loaf High (Figs. 3-4 and 6a-c). In the case of earlier anticline, a reactive diapir nucleates at its extensionally thinned crest (Figs. 6d-e and 7b). As they form over thick salt and with a relatively thin syn-kinematic overburden these reactive diapirs are highly symmetric (Jackson and Hudec, 2017).

5.3. Domain III: North edge of Sugar Loaf and Relay Zone 5.2.2.

Description

Domain III is located at the northern edge of the Sugar Loaf High where it connects downdip to the Tupi High by an ENE relay zone and to a smaller NE-oriented horst updip (Fig. 3). This domain is characterized by a change in the orientation and plan-form geometry of salt structures and minibasins. A 10 km wide NE-oriented salt wall (5, figs. 4 and 8), roughly rectangular in plan-view, occurs above this smaller pre-salt horst, having a sharp triangular edge to the south where it links with a different salt wall (3, fig. 4) by a narrow NW-oriented extensional salt ridge. Northwards, salt wall 5 branches out into two highly-curved and narrow (3-4 km) walls (Fig. 4). The western one (5a) trends NNW at the south and NE at the north, whereas the eastern wall (5b) trends NE at the south and NNE at the north. These walls have similar

profile geometries to walls in Domain II, with folding and upturn of a broadly tabular, highly faulted Albian section onlapped by Late Cretaceous-early Paleocene RSB strata, that is extended by inward-dipping growth faults at their edges (Wall 5, fig. 8). This indicates these walls have also a similar evolution to the ones in Domain II, with Late Cretaceous inflation/active diapirism followed by widening associated with reactive and passive rise during the remaining Late Cretaceous-Paleocene and RSB generation (Fig. 7).

Downdip of this Sugar-Loaf branch, a roughly rectangular, 8-10 km wide RSB forms above a base-salt basinward-dipping ramp, being limited downdip by a 6 km wide ENE-NE sigmoidal wall over the ENE-NE pre-salt relay zone (Wall 6, figs. 3-4). This wall shows signs of Late Cretaceous to Paleocene extension at its northern end, i.e. inward-dipping growth faults and a triangular reactive diapir nucleating above an anticline (Fig. 8a), and simultaneous shortening (folding) and inflation at its southeast flank (Fig. 8b-c).

Interpretation

At Domain III, over the Sugar-Loaf northern edge and near the ENE relay zone, deformation was driven by similar salt flux variations to Domain II (Figs. 6-8), resulting in wide passive/reactive walls and RSBs. However, their change in orientation and sigmoidal geometries in plan-view combined with asymmetric growth, suggest differential translation, plan-view rotation and shearing at the edge of the Sugar Loaf High and its smaller NE branches (Figs. 9-11).

As salt and cover translated downdip, reaching the Sugar-Loaf High and its updip NE branch, convergent salt flux resulted in thickening and pinning over the NE branch; whereas northwards, the system continued to translate unimpeded by any pre-salt

step (Fig. 9). This resulted in rotation and plan-view bending of the translational belt to the south where it became temporarily pinned and parallel to the pre-salt topography (Fig. 9). Physical models simulating gravity-driven translation across discontinuous pre-salt blocks illustrate how flow is radially channelized around these structures producing considerable rotation and shearing of salt walls at the edge of these blocks (Figs. 10a-b). Further basinward, a RSB formed by a combination of translation and clockwise rotation, as the system translated over the basinward-dipping ramp and eventually reached an ENE landward-dipping step downdip corresponding to the pre-salt relay zone (Figs. 8-9). There, initial inflation followed by widening and extension over the high (c.f. fig. 7) was coupled with gradual rotation and shearing in plan-view generating a sigmoidal wall that was also extended in the north away of the pre-salt high (wall 6, figs. 8-9).

5.4. Domain IV: West of Tupi

Description

North of the Sugar-Loaf and 20-50 km landward of the Tupi High, the trend of salt walls changes from N-NNE in the south (Domains II-III) to NE in Domain IV. Salt walls that extend northwards from Domains II-III bend up to 30° north-eastwards (walls 5 and 5a-b to 9 and 10, figs. 4). The salt walls in Domain are up to 30-50 km long, 5-8 km wide, and highly arcuate, with shorter (4-8 km long) and narrower (>1.5 km) NNW-NW-trending walls connecting the larger NE-oriented structures (Fig. 4).

NE-trending walls are up to 4.9 km tall with thin (c. 200-300 m) Albian growth strata showing abrupt thinning and direct onlaps towards the wall within a narrow halo of intense upturn at their flanks (walls 7-8, fig. 11a-b). Larger thickness variations occur associated with Upper Cretaceous to mid-Paleocene strata within c. 3 km thick

minibasins (Fig. 11). These strata can onlap an upturned Albian flap or directly onto the salt walls with abrupt cutoffs against them (Fig. 11a-b). The minibasins are generally characterized by vertically-aligned depocentres (i.e. bowls *sensu* Rowan and Weimer, 1998) and raised bathymetric rims implying they formed by density-driven subsidence (Hudec et al., 2009). In some cases, the minibasins are tilted, presenting a wedge-shaped mid-Paleocene section or asymmetric turtle anticline due to large salt evacuation and final welding below the minibasin, indicating the minibasins grounded during the early-mid Paleocene (*sensu* Rowan and Weimer, 1998) (Fig. 11a-b). These walls were also affected by mild extensional collapse during the Late-Paleocene-Neogene, although the basinwardmost wall (11), at the updip edge of the Tupi High kept growing by active rise and uplift (Fig. 11a-b).

The NW-oriented walls between walls 9 and 10 to the southwest near the boundary with Domain III are narrower (~ 1 km) and smaller (4-10 km long) than NE-oriented walls and terminate against them (Fig. 4). They are characterized by triangular geometries with inward-dipping and younging Upper Cretaceous to Paleocene normal growth faults (Fig. 11c). A wider (3 km) and taller (3.5 km) NW wall further north, broadly triangular in profile, connects walls 8 and 9 and presents a top-Albian local erosional unconformity on its SW flank denoting end of Albian active rise. Upper Cretaceous strata thin and onlap directly onto this wall without any visible faulting and Paleocene strata define a turtle anticline that is offset by inward-dipping and younging growth normal faults near the wall. Near the transition to Domain VI to the north, the area presents a polygonal pattern due to an earlier WNW-NW Albian trend characterized by narrow (> 1 km) and low-amplitude (> 250 m) anticlines within larger NE minibasins with growth synclines capped by a top-Albian unconformity (Figs. 4 and 11d)

Interpretation

Highly-upturned Albian growth strata at the flank of these walls constitute basal flaps that likely originated where the original salt contact dipped moderately, allowing a wedge of strata to directly onlap a gentle diapir (c.f. Rowan et al., 2016; Jackson and Hudec, 2017). This indicate an earlier, Albian phase of minor growth driven by halokinesis (passive and/or active rise) and late Albian burial followed by dismembering of a thin Albian roof by active rise during end of Albian-early Late Cretaceous. In places, Albian thickness variation can be also related to post-depositional structural thinning of highly-upturned flanks where there is no evidence of stratigraphic onlaps (W flank of wall 10, fig. 11b).

During the Late Cretaceous, after breaking through their thin Albian roof and reaching the surface, these walls experienced a long-lived phase of density-driven rise (i.e. downbuilding) until mid-Paleocene (Fig. 10a-d) (Jackson et al., 2014b; 2015). Basal Albian flaps on both sides of each wall are usually asymmetric, supporting that their growth was mainly driven by density-driven process (c.f. Rowan et al., 2016; Jackson and Hudec, 2017). Brief intermediate phases of active rise occurred by the end of the Cretaceous as seen by their relatively greater upturn and keystone normal faults (sensu Rowan et al., 1999) formed by outer-arc stretching at some of the diapir flanks (walls 8-9, fig. 11a-b). By mid-Paleocene, the walls became partially buried but continued growing by density-driven active rise (walls 7-8).

The downdip salt wall (10, fig. 11a-b) rises reactively to the north where it sits over a pre-salt high (Fig. 11a) and actively to the south where it lies landward of the same high, uplifting a c. 400m roof (Fig. 11b). In general, downdip walls near the Tupi High (9-11) are affected more and earlier by regional stresses (contraction and/or

extension), than walls further updip (7-8) (Figs. 11a-b). This occurs by development of inward-dipping normal growth faults at their sub-horizontal flanks indicating reactive rise (walls 10-11, fig. 11a); and normal faults associated with extensional collapse in the case of walls having limited salt supply and surrounded by welded minibasins (walls 8-9, figs.10a-b).

Along most of this domain, there are no major pre-salt structures and deformation is largely driven by density-driven subsidence and salt expulsion (Figs. 3 and 11). Nevertheless, ramp-syncline basins over the Sugar Loaf High to the south suggest that structures in Domain IV also translated downdip but without being significantly affected by pre-salt relief and, thus, not forming RSBs. As the structures progressively approached the Tupi High and its NNW-oriented northern branch, they started to be affected by plan-view differential flow and cross-sectional flux mismatches. Updip walls (7 and 8, fig. 11a-b) were less affected by lateral flux variations and deformation because they are farther (c. 50-60 km) of the Tupi High. Downdip salt walls (9-11, fig. 11a-b), however, present more variable trends and deformational history as they lie closer to the Tupi High and, thus, are influenced by late flux variations. NW-oriented extensional walls at the southern edge of this domain formed due to plan-view radial flow as structures flowed faster away of the Sugar Loaf High to the south (Figs. 3, 4 and 11c). Narrow NW-trending Albian anticlines within the large minibasins to the north indicate SW-directed shortening, which is probably associated with the concave margin geometry (c.f. Cobbold et al., 1995).

5.5. Domain V: Tupi High

Description

The Tupi High defines a gentle landward-dipping base-salt ramp updip that passes abruptly to a steep basinward-dipping edge downdip (Fig. 3 and 11a-b). The area is characterized by 30-40 km long and 2-4 km wide curvilinear salt walls and anticlines trending mainly NE-NNE with a dominant convex-to-basin planform (Fig. 4). Fewer and smaller NW walls extend across larger NE walls, being 5-10 km long and 1-2 km wide, apart from one 35 km long NW wall (Fig. 3-4).

Over the gentle landward-dipping base-salt ramp, NE-trending structures are predominantly characterized by low amplitude (c. 300m) salt anticlines, occasionally cored by intra-salt seaward-vergent shear zones, with a broadly tabular Albian roof folded and onlapped by Upper Cretaceous to Paleocene strata (Fig. 12a-b). 5-10 km further basinward, where base-salt topography flattens (Fig. 12b), similar salt anticlines have highly to completely dismembered roof due to normal faulting with Upper Cretaceous to mid-Paleocene growth strata, being occasionally pierced by reactive diapirs (Fig. 12a-b). These geometries suggest structures were originally formed by contraction as salt-cored buckle folds and later reactivated by extension.

Further basinward, 5-8 km near the crest of the Tupi High, new sets of salt-cored buckle folds affected by intra-salt shear zones and outer-arc extension appear where the base-salt relief steepens again (Fig. 12c). They have tabular Albian-early Upper Cretaceous roofs onlapped by thin Upper Cretaceous growth strata capped by a top Cretaceous unconformity (Fig. 12c). The tabular, pre-kinematic interval (white lines) becomes gradually thicker and younger landward (two westernmost growth synclines in fig. 12c) indicating contraction propagates landward from the crest of Tupi High. Folds nearer the Tupi crest are affected by greater lateral extension which results in roof dismembering and minor reactive rise (Fig. 11a-c). Folds located at the crest of the base-salt basinward-dipping ramp present open to monoclinal geometries with

flanks that are sub-parallel to the base-salt, extended by predominantly basinward-dipping normal faults and onlapped by Paleocene RSB strata (Fig. 12c-d).

Downdip of the Tupi High and over a set of closely-spaced tilted fault-blocks (Figs. 3-4), deformation is mainly characterized by salt-cored folds and associated Upper Cretaceous-Paleocene RSBs (Fig. 12a-e). The foldbelt is defined by narrow (1-2 km) and long (10-20 km) NE-oriented curvilinear folds with higher amplitude (500-700 m) and frequency (1-3 km) than the ones in Domain I and further updip (Figs. 4-5 and 11). The pre-kinematic interval consists mainly of tabular Albian strata, occasionally thinned by outer-arc extension and/or local erosional unconformities (Fig. 12a-e). Folds get generally tighter downdip of the Tupi High, and vergence varies more dramatically than in Domain I with seaward- and landward-vergent folds and thrusts being equally common (Fig. 12a-e).

Supra-salt thrusts form in the steeper flank of tighter anticlines and, in many cases, diapiric piercement occurs locally along their strike as a sliver of salt is carried up their hangingwall (thrust piercement, c.f. Hudec and Jackson, 2006) (Figs. 12a-e). Narrow (< 1 km) diapirs also form by squeezing and salt injection onto extensionally and/or erosionally thinned roofs of salt-cored folds (injection fold, c.f. Beloussov, 1959; Dooley et al., 2015; Jackson and Hudec, 2017) (Fig. 12d). These diapiric walls are also NE-oriented, being 10-20 km long and 1-2 km wide, narrower than in any other segment of the SPP (Fig. 4). Many of them are cored by intra-salt shear-zones and associated with intense upturn and structural thinning of sub-vertical Albian/Upper Cretaceous strata (Fig. 12a-d). In places, these walls develop small salt tongues by thrust piercement in their crest, which in cases can be double-vergent (Fig. 12d).

The general higher amplitude, narrowness and absence of inward-dipping normal growth faults on their flanks suggest these walls experienced little, if any, regional extension (Fig. 12), rising by renewed pulses of contraction during the Late Cretaceous/Paleocene. Earlier, Albian growth may have occurred locally but the related Albian onlaps and thickness changes are obscured by intense deformation and upturn in the flank of these walls (Fig. 12). The Upper Cretaceous-Paleocene main growth interval is characterized by predominantly landward onlapping and thickening strata defining ramp-syncline basins (RSBs, Pichel et al., 2018a), which, in places, are stacked due to translation over multiple base-salt ramps (Fig. 12d-e). NW walls form at the edges of NE folds and/or where salt walls converge along-strike (Fig. 4). They are located within base-salt lows and characterized by stacked seaward-vergent reverse shear zones and thicker salt (c. 2.5 km) than the adjacent NE salt structures (c. 2 km thick), which indicate greater Late Cretaceous/Paleocene contraction (Fig. 12c and f).

Interpretation

The foldbelt and general style of diapirism and RSBs is consistent with models of basinward translation over sets of gentle landward-dipping and steep basinward-dipping base-salt ramps (Fig. 13a). Convergent salt flux and buttressing over a gentle landward-dipping step resulted in contraction and a landward-younging fold-belt (Fig. 12a-c and 13a); and where this step passed to a ~5 km base-salt flat, these early folds were mildly extended (Fig. 13a).

Over the Tupi basinward-dipping edge, the cross-sectional area of salt arriving at its crest was smaller than the one leaving producing a flux mismatch, cover subsidence and development of a topographic monocline over the associated base-salt ramp

(Figs. 12 and 13a). This monocline was characterized by extension at the top of the ramp and contraction at its base while being filled with sediments that were continuously translated basinward forming a ramp-syncline basin (Fig. 12 and 13a). Extension over the Tupi crest unfolded and/or extended earlier salt anticlines formed updip but is minor compared to the degree of contraction, thrusting and diapir squeezing downdip (Fig. 12 and 13a). This occurred because a set of narrow, closely-spaced pre-salt fault-blocks (Fig. 3) produced abrupt flux variations and additional buttressing, resulting in renewed pulses of contraction that overprint updip extension as structures moved across them (Fig. 13a). This generated a series of squeezed diapirs, folding amplification, thrust piercement and diapir injection on the core of earlier folds (Figs. 12 and 13a).

The presence of NW-oriented walls showing higher degree of contraction and amplitude than adjacent NE-oriented walls and located over base-salt lows (Fig. 12c and f) suggests flow was radially channelized around smaller, discontinuous pre-salt structures (Fig. 13b). This is explained by the concave plan-view geometry of the Tupi High downdip edge and the presence of a large, roughly rectangular pre-salt horst downdip from its centre (Figs. 3 and 13b). As salt anticlines translated from the Tupi High they were pinned behind this horst, converging and, thus coalescing and producing thicker NW-oriented ridges, whilst rotating and diverging away of it to the sides (Figs. 13b), similar to results from physical models (Fig. 10a-b) (Dooley et al., 2018).

5.6. Domain VI: NNW branch and N of Tupi

Description

Domain VI lies immediately to the north of Tupi, above and downdip of its NNW-oriented horst-like branch (Fig. 3), being dominantly characterized by NNE-oriented salt anticlines and walls with a few WNW-oriented salt walls (Figs. 3-4). The structural pattern becomes progressively more polygonal to the north, away from the pre-salt highs, with an increased presence of WNW- and NW-trending salt walls (Fig. 4). Both the NNE- and WNW-oriented diapiric walls demonstrate gradual thinning and onlap of Albian strata towards the walls and Top-Albian local unconformities at their flanks, indicating an early, Albian phase of growth (Fig. 14). WNW anticlines occur within the larger minibasin to the west having similar geometries and dimensions to Albian anticlines in the adjacent domain IV, indicating SW-oriented Albian shortening (see section 5.4, figs. 4 and 11d). This shows a strong link between the polygonal framework north of the area and an earlier, Albian growth phase in Domains IV and VI.

Landward, above the NNW-trending pre-salt high, the structural style is dominated by wide (3-5 km) NNE-oriented triangular salt walls whose roofs are cut by numerous inward-dipping and inward-younging normal faults (Fig. 14a). The walls have gentle to moderately-dipping flanks extended by growth faults during Late Cretaceous-early Paleocene, indicating they formed by extension and reactive diapirism (Fig. 14a). As these reactive walls are limited basinward by c. 500 m thick RSBs of same age (Fig. 14a), extension occurred in tandem with translation after an initial phase of inflation/active rise during the Albian-Late Cretaceous (Fig. 14a). Over the pre-salt high basinward-dipping edge, an early Paleocene anticline and a salt wall uplift and fold an Upper Cretaceous RSB whilst being onlapped by early Paleocene RSB strata (stacked RSBs, c.f. Pichel et al., 2018a) indicating early Paleocene contraction (Fig. 14a).

Further basinward, downdip of the NNW pre-salt high, the deformation style is notably different, being represented by a 30 km wide NNE-NE fold-belt. These folds also differ from WNW folds further updip as their main growth phase occurred during the Late Cretaceous-Paleocene, as seen by a broadly isopachous Albian interval onlapped by Upper Cretaceous-Paleocene asymmetric, sigmoidal strata (i.e. RSBs, Fig. 14a). Local top-Albian unconformities in few of these folds, however, suggest earlier minor growth during the Albian (Fig. 14a). The relationship with pre-salt relief and architecture of this fold-belt are similar to Domain V (Fig. 12-13a), although the degree of intra-salt shearing, diapir squeezing and thrusting is markedly less; indicating less shortening and resulting in fewer salt walls rising diapirically from the top of anticlines (Fig. 14a).

Northwards, away from pre-salt highs, walls have higher amplitudes (2-3 km), being surrounded by equally thick, nearly-welded minibasins with highly upturned Albian to Upper Cretaceous strata onlapping directly onto the wall and with drastic thickness variations (Fig. 14c). Less upturned Paleocene strata onlap an Upper Cretaceous carapace, showing progressively less thickness variations and covering the diapir (Fig. 14b). The walls are also affected by Late Cretaceous-Paleocene normal faults, which form predominantly at the flank of triangular diapirs and are associated with local syn-depositional growth (i.e. strata below regional) indicating lateral extension (Fig. 14b). However, in cases where they occur over the wall crest and above regional without growth strata, they are be purely related to outer-arc stretching indicating roof uplift and bending driven by active diapirism (Fig. 14b). Few younger, Neogene normal faults also form by diapir collapse (Fig. 14b) as elsewhere in the study-area. These characteristics indicate deformation is mainly controlled by density-driven processes; with early stage downbuilding followed by halokinetic

active rise as the walls become partially buried during the Paleocene (Fig. 14b). This structural signature increases northwards, away of pre-salt highs, probably, contributing to the polygonal pattern observed in the area (Fig. 3-4 and 13).

Interpretation

As elsewhere in the study-area structures translated downdip as seen by the occurrence of large RSB systems in this Domain and further south in Domain V (Figs 11 and 13). To the south of Domain VI, translation and development of salt structures were largely influenced by the NNW branch of the Tupi High (Fig. 14a), whereas northwards, away of this pre-salt high, structures were mainly driven by density-driven processes (Fig. 14b).

Over this horst-like NNW branch of Tupi, movement over a steep landward-dipping edge resulted in similar growth pattern to the updip edge of the Domain II (Fig. 6-7 and 14a). However, as this high and its correspondent base-salt flat were narrower, extension and widening of initially inflated walls were relatively less than in Domain II (Figs. 6 and 14). This resulted in 5-6 km wide reactive walls limited immediately downdip by RSBs (Fig. 14a). Further basinward, a new set of RSBs formed over the pre-salt high basinward-dipping ramp and an associated contractional fold-belt formed as the system translated and decelerated over a base-salt contractional hinge at the base of the ramp (Fig. 14a) (c.f. Dooley et al., 2017), similar to Domain V (Figs. 12-13a). This structural pattern is remarkably similar to models of translation over a pre-salt horst (Fig. 1d) (Dooley et al., 2017; Pichel et al., 2018a,b). Contraction was less than Domain V further south, not producing highly squeezed structures due to the lack of closely-spaced pre-salt steps (Fig. 3, 14a). Despite c. 30 km of translation in the area (Pichel et al., 2018a), increased density-driven

subsidence and downbuilding northwards is attributed to initially thicker salt over the pre-salt low (c.f. Davison et al., 2012; Rodriguez et al., 2018) and lesser influence of base-salt relief and related flux variations away of pre-salt highs.

6. Discussion

6.1. Regional Kinematics and Structural Style Distribution

The main phase of deformation and diapirism in the SPP occurs during the Late Cretaceous to mid-Paleocene as evidenced by greatest thickness variations, faulting, folding and unconformities of same age around diapirs and minibasins (Gamboa et al., 2008; Davison et al., 2012; Fiduk and Rowan, 2012; Guerra and Underhill, 2012; Jackson et al., 2015) (Figs. 5-14). However, at least an earlier phase of post-depositional growth occurs during the Albian (Fig. 4) and a few authors suggest that a syn-depositional Aptian phase may also have occurred (Davison et al., 2012; Quirk et al., 2012). Additionally, Eocene-Neogene diapir fall (roof collapse over normal faults with associated salt horns in figs. 6, 8 and 11), dissolution (flat-topped walls, see Rodriguez et al., 2018), and local active rise of narrow walls (fig. 6a and 8a) are also observed. Here, we discuss the kinematics and mechanisms controlling these main phases of deformation.

6.1.1. Early Deformation Stages

Aptian syn-depositional growth in the SPP has been subject of intense debate (Davison et al., 2012; Quirk et al., 2012; Jackson et al., 2015a,b). Evidence of major growth are ambiguous as many intra-salt thickness variations, truncations and complex deformation patterns can be also attributed to post-depositional salt flow and strain portioning across multiple intra-salt detachments (see Albertz and Ings,

2012; Cartwright et al. 2012; Fiduk and Rowan, 2012; Dooley et al., 2015; Jackson et al., 2015b).

Albian deformation occurs predominantly in the north of the study-area, in Domains IV and VI (Figs. 7 and 9a), associated with WNW-NW and NNE-NE salt walls and anticlines resulting in an early polygonal pattern in these areas (Fig. 4). Albian movement also occurs in Domains I-III, locally along larger NNE-oriented walls and NW salt anticlines (Fig. 4). Although interpretation of the deeper Albian structures is complicated by multiphase Late-Cretaceous-Paleocene deformation, the NNE-NE Albian salt walls can be attributed to inflation and/or contraction in response to the well-documented SE-oriented updip extension (c.f. Guerra and Underhill, 2012; Quirk et al., 2012; Davison et al., 2012). The origin of the WNW-NW Albian trend and, thus, the polygonal framework north of the area, however, remains subject of debate. Some authors suggest it is related to an Eocene switch in sediment input (Guerra and Underhill, 2012), whereas others suggest Late Cretaceous convergent gliding due to the concave shape of the margin (Cobbold et al., 1995) (Fig. 1b and 15a).

As the locus of greater Albian movement and polygonal pattern occurs at the northern and north-eastern edges of the data-set (Domains IV and VI), north-northeast of the Tupi High, their triggers may lie outside of our study-area. Thus, we integrate structures maps from previous studies (Guerra and Underhill, 2012) comprising an area immediate northwards of our study-area to understand the origin of this oblique and enigmatic WNW Albian trend. These maps show the existence of WNW to W-E linear, low-relief salt ridges associated with salt rollers in the extensional domain, updip of the CFF defining the Albian Gap (Fig. 15b-c) (c.f. Guerra and Underhill, 2012). These ridges pass downdip to higher-amplitude salt

walls with variable orientation and WNW-, W-E and ENE-trending ridges within larger minibasins (Fig. 15c), as the Albian contractional anticlines identified in Domains IV and VI (Fig. 11d). This suggests both sets of structures were formed during the Albian by S-SW-oriented contraction due to the E-W margin segment and its concave geometry (Fig. 15).

6.1.2. Late Cretaceous-Paleocene Deformation

The main deformation phase of the SPP (Late-Cretaceous-Paleocene) has been subject of a large controversy (see section 1). The distribution, orientation and geometry of age-equivalent salt-cored buckle-folds in Domains I and V-VI are unequivocal evidence of Late Cretaceous/Paleocene shortening (Quirk et al., 2012; Guerra and Underhill, 2012; Fiduk and Rowan, 2012; Jackson et al., 2015b). However, these fold-belts are separated by domains (II-IV) with remarkably different diapir and minibasin geometries that are mainly associated with translation, extension and/or differential loading (Figs. 6-11). This indicates that shortening was not a widespread phenomenon as suggested by some workers (e.g. Quirk et al., 2012; Guerra and Underhill, 2012; Fiduk and Rowan 2012; Alves et al., 2017), being focused over base-salt landward-dipping ramps and downdip of basinward-dipping ramps (Figs. 4-13).

Evidence of at least three modes of diapirism (passive, reactive and active, see Vendeville and Jackson, 1992a; Hudec and Jackson 2007) are ubiquitous in the study-area (Figs. 5-13). Over pre-salt highs (Sugar Loaf and Tupi), deformation is dominated by extension, with reactive and passive diapir rise and/or extensional collapse, following a brief, early phase of contraction (Fig. 6, 7, 12 and 14). At the edge of pre-salt structures, deformation is characterized by rotation, radial flow and

map-view shearing (Figs. 8-10 and 13b); whereas away of pre-salt highs deformation is dominated by density-driven processes (Fig. 11).

These observations coupled with the existence of multiple RSBs (Figs. 6, 8, 12 and 14) (Pichel et al., 2018a), and the predominance of linear salt features parallel to the nearby base-salt relief (Figs. 3-4) indicate that the bulk of deformation in the SPP was driven by translation and associated salt flux variations caused by initial salt thickness contrasts across base-salt relief (Figs 7, 9 and 13).

6.1.3. Salt Flow patterns

Salt and overburden translation and the associated flux mismatches are driven primarily by viscous shear drag (i.e. Couette flow, c.f. Weijermars et al., 1993; 2014; Rowan et al., 2004) within the salt (Fig.16a) (Dooley et al., 2017; Pichel et al., 2018a). In this case, salt streamlines (c.f. Dooley et al., 2017) can converge over base-salt step-ups and diverge over step-downs producing, respectively, thickening and thinning of the flow section (Fig. 16a). Thin salt regions are more resistive to flow whereas thick salt regions are less resistive, resulting in faster overburden movement where salt is thicker and slower movement where salt is thinner. This ultimately produces zones of inflation and contraction at the updip edge of pre-salt highs and zones of subsidence (monoclines) with hinges producing updip extension and downdip contraction at the downdip edges of pre-salt highs (Fig. 16a) (Dooley et al., 2017) as observed in the SPP (Figs. 5-14).

This is, nonetheless, an idealized flow profile as, in nature, salt flow is typically more complex and hybrid (Weijermars et al. 2014; Jackson and Hudec, 2017), evolving through time (Fig. 16b-c). In the case of a thick, mechanically layered salt such as that present in the SPP, flow is expected to be even more complex due to intra-salt

rheological variability and mechanical layering (c.f. Cartwright et al., 2012; Jackson et al., 2015b). The salt in the SPP is notably rich in bittern-salts which correspond to 15-35% of the composition of the most reflective intra-salt intervals (Rodriguez et al., 2018). These bittern salts and are up to 10^6 times less viscous and flow 10^{2-5} times faster than halite (Van Keken et al., 1993; Jackson and Hudec, 2017); thus affording multiple highly-lubricant intra-salt detachments and strong flow partition in the area.

This is seen in physical models simulating downdip flow of a mechanically-layered salt section tilted basinward (Figs. 16b-c). At the early stages, when the suprasalt roof is of negligible thickness, first-order salt flow is driven by viscous shearing of the whole salt column following a typical Couette flow profile (Fig. 16b). Second-order flow within each discrete mobile interval (black) separated by more competent layers (coloured layers) is however more complex, varying from a typical Poiseuille flow profile (c.f. Rowan et al., 2004) at the lowermost level to hybrid, albeit Couette-dominated flow upward (Fig. 16b). This is seen in the SPP, where the entire salt section is being sheared basinward and deforming primarily by Couette-flow as the salt and overburden translate downdip; whereas the lowermost, halite-rich level has been expelled and inflated without significant shearing (Fig. 5-14). In the later stages of translation, as the overburden gradually thickens and becomes more resistant to translation, flow becomes more hybrid, with most discrete salt intervals following a Poiseuille-flow pattern, although the first-order flow remains predominantly Couette (Fig. 16c).

6.2. Implications for the origin of the Albian Gap

Bulk translation (c. 30 km, Pichel et al., 2018) started by the end of Albian and continued until approximately mid-Paleocene. Salt and overburden moved across

pre-salt structures and base-salt steps in response to SE-directed salt flow (Pichel et al., 2018). These base-salt steps perturbed flow resulting in localized extension and shortening generating a series of RSBs and complex diapirism. In gravity-driven kinematically-linked systems an intermediate zone of translation links domains of updip extension and downdip contraction and/or salt advance (Rowan et al., 2004; Hudec and Jackson 2007; Jackson et al., 2015a, Peel 2014b, Allen et al., 2016). Thus, c. 30 km of Late Cretaceous-Paleocene basinward (i.e. SE) translation must be balanced by similar amounts of coeval updip extension and downdip contraction or salt advance (Rowan et al., 2004; Peel 2014b; Jackson et al., 2015a). Consequently, this helps understanding the regional kinematics of the Central Santos Basin and, specially, the origin of the enigmatic Albian Gap.

Previous studies (Davison et al., 2012; Quirk et al 2012; Jackson et al., 2015a,b) recognized the existence of an approximately 30 km wide salt nappe along most of the downdip edge of the Santos Basin (Fig. 1b-c). This salt nappe is estimated to have formed by the end of the Albian to Late Cretaceous (Davison et al., 2012), thus roughly balancing our bulk translation estimates in the SPP (Pichel et al., 2018a). Updip extension is well documented as an array of salt-detached listric normal faults, salt rollers and reactive diapirs formed during the Albian, thus pre-RSBs (Guerra and Underhill, 2012, Davison et al., 2012, Quirk et al., 2012). This zone passes downdip to the Albian Gap, where c. 60 km of Albian section is separated by a large basinward-dipping Upper Cretaceous-Paleocene rollover before reaching the SPP (Fig. 2) (Jackson et al., 2015a).

Much work has been published on the enigmatic Albian Gap. Some authors suggest the structure was driven primarily by Late Cretaceous/Paleocene extension which generated a unique and remarkably large, 60 km landward-dipping listric fault (i.e.

Cabo Frio Fault; CFF) (Guerra and Underhill, 2012, Davison et al., 2012, Mohriak et al., 2012; Quirk et al., 2012). Other authors (Ge et al., 1997; Gemmer et al., 2004; Jackson et al., 2015a, Jackson and Hudec, 2017) suggest the Albian Gap was already in existence by the end of Albian as an equally impressive 60 km wide salt wall, and that Late Cretaceous-Paleocene expulsion produced the basinward-dipping rollover and salt inflation in the SPP.

Based on our recognition of Late Cretaceous-Paleocene RSBs recording c. 30 km of SE-oriented translation and the multiphase style of diapirism in the SPP, combined with the Albian Gap rollover geometry (c.f. Jackson et al., 2015a), we propose a new model for the origin of the enigmatic Albian Gap (Fig. 17). Our model shows that Albian extension led to the development of c. 30 km wide salt wall that reached the Albian paleo-sea-floor (Fig. 17a-b), similar albeit half the size than what was proposed by Jackson et al. (2015a). This wall was deflated and extended additional 30 km during the Late Cretaceous-Paleocene indicating a combination of roughly coeval salt expulsion (density-driven subsidence) and lateral extension (Fig. 17b-c). This resulted in salt being expelled seaward onto the SPP, development of c. 30 km wide landward-dipping listric normal fault (CFF) and the current 60 km wide Albian Gap (Fig. 17c). In summary, our analysis suggests the Albian Gap formed by a combination of processes; at least 30km of Late Cretaceous-Paleocene extension must have occurred in order to balance the downdip translation in the SPP (Fig. 17c). The other 30km of the gap may be explained by earlier, Albian extension (Fig. 17d) and/or as an original depositional gap over an inflated salt high.

7. Conclusions

This study contributes to the long-lived debate regarding the controversial evolution of the Central Santos Basin, elucidating the mechanisms and regional deformational styles of the São Paulo Plateau as well as the Albian Gap. The kinematics, geometries, orientation and distribution of salt structures and minibasins, and their relationship with base-salt structures confirms that salt tectonics in the São Paulo Plateau was controlled by non-uniform basinward translation of thick, layered salt over base-salt relief. Viscous salt drag over prominent basal topography generated salt flux variations due to initial thickness contrasts across base-salt steps that resulted in complex distribution and composite growth patterns of salt structures and development of ramp-syncline basins. Structures and minibasins landward of the main base-salt steps presented a simpler evolution dominated by density-driven processes with more random orientation and less kinematic variations. At the edge of pre-salt highs or around discontinuous structures, deformation was characterized by rotation, plan-view shearing and radial flow.

Ramp-syncline basins and the variable, multiphase style of salt deformation associated with them demonstrate that c. 30 km of translation occurred in the São Paulo Plateau during the Late Cretaceous-Paleocene. This value can be extrapolated to neighbouring structural domains and, therefore, help understanding the kinematics of the controversial Albian Gap updip. We propose that the 50-60 km wide gap formed by a combination of lateral extension and salt expulsion, with 20-30 km of Albian extension followed by 30 km of Late Cretaceous-Paleocene extension, balancing the synchronous 30 km of translation downdip. Late Cretaceous-Paleocene extension occurred in tandem with salt expulsion of an early-formed 20-30 km wide salt wall to generate the dramatic basinward-rollover geometry associated with it. The concepts presented here can improve the comprehension of

complex salt-related deformation through time and space in various salt basins affected by thin-skinned gravity-driven deformation and translation above a dipping and irregular salt detachment.

Acknowledgements

The authors wish to thank Mads Huuse, Mike Hudec, Oliver Duffy, Mark Rowan and Gillian Apps for the fruitful discussions and constructive criticism. We thank CGG for providing access to the high-quality 3D seismic dataset used in this study and WesternGeco for the PSDM 2D transects. The main author would also like to thank the Science without Borders program and CNPq, Brazil for sponsoring his PhD research. Schlumberger is also acknowledged for provision of Petrel software.

References

Albertz, M., & Ings, S. J., 2012. Some consequences of mechanical stratification in basin-scale numerical models of passive-margin salt tectonics. Geological Society, London, Special Publications, 363(1), 303-330.

Allen, H., Jackson, C. A. L., Fraser, A. J., 2016. Gravity-driven deformation of a youthful saline giant: the interplay between gliding and spreading in the Messinian basins of the Eastern Mediterranean. Petroleum Geoscience, 22(4), 340-356.

Alves, T. M., Fetter, M., Lima, C., Cartwright, J. A., Cosgrove, J., Gangá, A, Strugale, M., 2017. An incomplete correlation between pre-salt topography, top reservoir erosion, and salt deformation in deep-water Santos Basin (SE Brazil). Marine and Petroleum Geology, 79, 300-320.

Beloussov, V. V., 1959. Types of folding and their origin. International Geology Review, 1(2), 1-21.

Brown, A. R., 2011. Interpretation of three-dimensional seismic data. Society of Exploration Geophysicists and American Association of Petroleum Geologists.

Brun, J. P., Fort, X., 2011. Salt tectonics at passive margins: Geology versus models. Marine and Petroleum Geology, 28(6), 1123-1145

Cartwright, J., Jackson, M., Dooley, T., Higgins, S., 2012. Strain partitioning in gravity-driven shortening of a thick, multilayered evaporite sequence. Geological Society, London, Special Publications, 363(1), 449-470.

Contreras, J., Zühlke, R., Bowman, S., Bechstädt, T., 2010. Seismic stratigraphy and subsidence analysis of the southern Brazilian margin (Campos, Santos and Pelotas basins). Marine and Petroleum Geology, 27(9), 1952-1980.

Cobbold, P. R., Szatmari, P., Demercian, L. S., Coelho, D., Rossello, E. A. (1995). Seismic and experimental evidence for thin-skinned horizontal shortening by convergent radial gliding on evaporites, deep-water Santos Basin, Brazil, *in*: Jackson, M. P. A., Roberts, D. G., Snelson, S. (eds) Salt tectonics: a global perspective. AAPG Memoir 65, 305-321.

Demercian, S., Szatmari, P., Cobbold, P. R., 1993. Style and pattern of salt diapirs due to thin-skinned gravitational gliding, Campos and Santos basins, offshore Brazil. Tectonophysics, 228(3-4), 393-433.

Davison, I., Anderson, L., Nuttall, P., 2012. Salt deposition, loading and gravity drainage in the Campos and Santos salt basins. Geological Society of London Special Publications, 363(1), 159-174.

Dooley, T. P., Jackson, M. P., Jackson, C. A. L., Hudec, M. R., Rodriguez, C. R., 2015. Enigmatic structures within salt walls of the Santos Basin—Part 2: Mechanical explanation from physical modelling. Journal of Structural Geology, 75, 163-187.

Dooley, T. P., Hudec, M. R., Carruthers, D., Jackson, M. P., Luo, G., 2016. The effects of base-salt relief on salt flow and suprasalt deformation patterns—Part 1: Flow across simple steps in the base of salt. Interpretation, 5(1), SD1-SD23.

Dooley, T. P., Hudec, M. R., 2016. The effects of base-salt relief on salt flow and suprasalt deformation patterns—Part 2: Application to the eastern Gulf of Mexico. Interpretation, 5(1), SD25-SD38.

Fiduk, J. C., Rowan, M. G., 2012. Analysis of folding and deformation within layered evaporites in Blocks BM-S-8 &-9, Santos Basin, Brazil. Geological Society, London, Special Publications, 363(1), 471-487.

Gamboa, L.A.P., Machado, M.A.P., Silveira, D.P., Freitas, J.T.R., Silva, S.R.P., 2008. Evaporitos estratificados no Atlântico Sul: interpretação sísmica e controle tectono-estratigráfico na Bacia de Santos. In: W. Mohriak, P. Szatmari & S. M. C. Anjos (Org.), Sal: Geologia e Tectônica. Editora Beca, São Paulo, 2ed., p. 343-361.

Ge, H., Jackson, M. P., Vendeville, B. C., 1997. Kinematics and dynamics of salt tectonics driven by progradation. AAPG bulletin, 81(3), 398-423.

Gemmer, L., Ings, S.J., Medvedev, S. Beaumont, C., 2004. Salt tectonics driven by differential sediment loading: stability analysis and finite-element experiments. Basin Research, 16(2), 199-218.

Guerra, M. C., Underhill, J. R., 2012. Role of halokinesis in controlling structural styles and sediment dispersal in the Santos Basin, offshore Brazil. Geological Society, London, Special Publications, 363(1), 175-206.

Hudec, M. R., Jackson, M. P. A., 2004. Regional restoration across the Kwanza Basin, Angola: Salt tectonics triggered by repeated uplift of a metastable passive margin. AAPG bulletin, 88(7), 971-990.

Hudec, M. R., Jackson, M. P., 2006. Advance of allochthonous salt sheets in passive margins and orogens. AAPG bulletin, 90(10), 1535-1564.

Hudec, M. R., Jackson, M. P., 2007. Terra infirma: Understanding salt tectonics. Earth-Science Reviews, 82(1), 1-28.

Hudec, M. R., Jackson, M. P., Schultz-Ela, D. D. 2009. The paradox of minibasin subsidence into salt: Clues to the evolution of crustal basins. Geological Society of America Bulletin, 121(1-2), 201-221.

Jackson, M. P. A., Hudec, M. R., Fraenkl, R., Sikkema, W., Binga, L., Da Silva, J. 2001. Minibasins translating down a basement ramp in the deepwater monocline province of the Kwanza Basin, Angola [abs.]. In: American Association of Petroleum Geologists Annual Meeting Official Program, 10, A99.

Jackson, M. P., Hudec, M. R., 2005. Stratigraphic record of translation down ramps in a passive-margin salt detachment. Journal of Structural Geology, 27(5), 889-911.

Jackson, M.P., Hudec, M.R., 2017. Salt Tectonics: Principles and Practice. Cambridge University Press.

Jackson, C. A., Jackson, M. P., Hudec, M. R., Rodriguez, C., 2014a. Internal structure, kinematics, and growth of a salt wall: Insights from 3-D seismic data. Geology, 42(4), 307-310.

Jackson, C. A. L., Rodriguez, C. R., Rotevatn, A., Bell, R. E., 2014b. Geological and geophysical expression of a primary salt weld: An example from the Santos Basin, Brazil. Interpretation, 2(4), SM77-SM89.

Jackson, C. A. L., Jackson, M. P., Hudec, M. R., 2015a. Understanding the kinematics of salt-bearing passive margins: A critical test of competing hypotheses for the origin of the Albian Gap, Santos Basin, offshore Brazil. Geological Society of America Bulletin, 127(11-12), 1730-1751.

Jackson, C. A. L., Jackson, M. P., Hudec, M. R., Rodriguez, C. R. 2015b. Enigmatic structures within salt walls of the Santos Basin—Part 1: Geometry and kinematics from 3D seismic reflection and well data. Journal of Structural Geology, 75, 135-162.

Karner, G. D., Gambôa, L. A. P., 2007. Timing and origin of the South Atlantic pre-salt sag basins and their capping evaporites. Geological Society, London, Special Publications, 285(1), 15-35.

Krézsek, C., Adam, J. and Grujic, D., 2007. Mechanics of fault and expulsion rollover systems developed on passive margins detached on salt: insights from analogue modelling and optical strain monitoring. Geological Society, London, Special Publications, 292(1), pp.103-121.

Marton, G., Tari, G. Lehmann, C., 1998. Evolution of salt-related structures and their impact on the post-salt petroleum systems of the Lower Congo Basin, offshore

Angola. In: American Association of Petroleum Geologists International Conference and Exhibition, Rio de Janeiro. Extended Abstracts Volume, 834–834.

Meisling, K. E., Cobbold, P. R., Mount, V. S., 2001. Segmentation of an obliquely rifted margin, Campos and Santos basins, southeastern Brazil. AAPG bulletin, 85(11), 1903-1924.

Modica, C. J., Brush, E. R., 2004. Postrift sequence stratigraphy, paleogeography, and fill history of the deep-water Santos Basin, offshore southeast Brazil. AAPG bulletin, 88(7), 923-945.

Mohriak, W.U., Macedo, J.M., Castellani, R.T., Rangel, H.D., Barros, A.Z.N., Latgé, M.A.L., Mizusaki, A.M.P., Szatmari, P., Demercian, L.S., Rizzo, J.G. Aires, J.R. (1995). Salt tectonics and structural styles in the deep-water province of the Cabo Frio region, Rio de Janeiro, Brazil, *in*: Jackson, M. P. A., Roberts, D. G., Snelson, S. (eds) Salt tectonics: a global perspective. AAPG Memoir 65, 273-304.

Mohriak, W., Nemčok, M., Enciso, G., 2008. South Atlantic divergent margin evolution: rift-border uplift and salt tectonics in the basins of SE Brazil. Geological Society, London, Special Publications, 294(1), 365-398.

Mohriak, W.U., Szatmari, P., Anjos, S.M.C., 2009. Sal: Geologia e Tectônica. Editora Beca, São Paulo,450 pp

Mohriak, W. U., Szatmari, P., Anjos, S., 2012. Salt: geology and tectonics of selected Brazilian basins in their global context. Geological Society, London, Special Publications, 363(1), 131-158.

Peel, F., Jackson, M.P. Ormerod, D., 1998 Influence of Major Steps in the Base of Salt on the Structural Style of Overlying Thin-skinned Structures in Deep Water

Angola, American Association of Petroleum Geologists International Conference and Exhibition, Rio de Janeiro, Brazil, November, Extended Abstracts Volume, pp. 366-367.

Peel, F. J., 2014b. The engines of gravity-driven movement on passive margins: Quantifying the relative contribution of spreading vs. gravity sliding mechanisms. Tectonophysics, 633, 126-142.

Pichel, L.M., Peel, F., Jackson, C.A.-L., Huuse, M., 2018, Geometry and kinematics of salt-detached ramp syncline basins, Journal of Structural Geology, 115, 208-230. in press, doi: 10.1016/ j.jsg.2018.07.016.

Pichel, L. M., Finch, E., Gawthorpe, R., 2018b. Impacts of Pre-salt Rift Topography on Salt Tectonics

Quirk, D. G., Schødt, N., Lassen, B., Ings, S. J., Hsu, D., Hirsch, K. K., Von Nicolai, C., 2012. Salt tectonics on passive margins: examples from Santos, Campos and Kwanza basins. Geological Society, London, Special Publications, 363(1), 207-244.

Rodriguez, C. R., Jackson, C. L., Rotevatn, A., Bell, R. E., Francis, M., 2018. Dual tectonic-climatic controls on salt giant deposition in the Santos Basin, offshore Brazil. Geosphere, 14(1), 215-242.

Rowan, M. G., Weimer, P., 1998. Salt-sediment interaction, northern Green Canyon and Ewing bank (offshore Louisiana), northern Gulf of Mexico. AAPG bulletin, 82(5), 1055-1082.

Rowan, M. G., Jackson, M. P., Trudgill, B. D., 1999. Salt-related fault families and fault welds in the northern Gulf of Mexico. AAPG bulletin, 83(9), 1454-1484.

Rowan, M. G., Trudgill, B. D., Carl Fiduk, J., 2000. Deep-Water, Salt-Cored Foldbelts: Lessons from the Mississippi Fan and Perdido Foldbelts, Northern Gulf of Mexico. Atlantic rifts and continental margins, 173-191.

Rowan, M. G., Peel, F. J., & Vendeville, B. C. (2004). Gravity-driven fold belts on passive margins.

Rowan, M. G., Giles, K. A., Hearon IV, T. E., Fiduk, J. C., 2016. Megaflaps adjacent to salt diapirs. AAPG Bulletin, 100(11), 1723-1747.

Van Keken, P.E., Spiers, C.J., Van den Berg, A.P. and Muyzert, E.J., 1993. The effective viscosity of rocksalt: implementation of steady-state creep laws in numerical models of salt diapirism. Tectonophysics, 225(4), pp.457-476.

Vendeville, B. C., Jackson, M. P. A., 1992a. The rise of diapirs during thin-skinned extension. Marine and Petroleum Geology, 9(4), 331-354.

Weijermars, R., Jackson, M. P., Dooley, T. (2014). Predicting the depth of viscous stress peaks in moving salt sheets: Conceptual framework and implications for drilling Viscous Stress Peaks in Moving Salt Sheets. AAPG bulletin, 98(5), 911-945.

Figure Captions

Figure 1: (a) Schematic cross-sections demonstrating classical distribution and style of gravity-driven salt tectonics along continental margins, with an updip extensional domain passing downdip to an intermediate and undeformed translational province and a downdip shortening domain (adapted from Jackson et al., 2015a). (b) Schematic cross-sections based on physical models showing the effects of base-salt relief and thickness variations on salt flow and overburden deformation (after Dooley et al., 2017). (c) Location map of the study-area, the São Paulo Plateau, Central Santos Basin Brazil with the main salt-related structural provinces indicated. Our 3D seismic survey is highlighted in red and other previous studies location in polygons with different colours. Black line is the location of the geoseismic section presented in (d) showing the main structural elements of the study-area, with the Albian gap updip, passing downdip to a zone of thickened salt over complex and prominent base-salt topography of the Tupi Sub-High, and further downdip to a frontal salt nappe.

Figure 2: Uninterpreted and interpreted regional PSDM line showing the main salt-related structural elements of the Central Santos Basin: an updip extensional domain, a c. 60km of

Albian Gap, The São Paulo Plateau (SPP) and a deep-salt basin domain characterized by high-amplitude, squeezed diapirs and allochthonous salt sheets. The base-salt geometry is characterized by a series of landward- and basinward-dipping base-salt ramps up to 2 km associated to rift normal faults that generate drape folds on the base-salt and/or small offsets (location in fig. 1, 3 and 4).

Figure 3: Static-corrected base-salt structure map illustrating the main base-salt highs and associated steps in (a), and overlay of different structural domains of the SPP and location of sections presented in this study in (b). The black polygon in (a) corresponds to the location of the depth bas-salt structure map adapted from Alves et al. (2017) for comparison.

Figure 4: (a) TWT top-salt structure map showing the framework of salt walls and minibasins oriented predominantly NNE orientation but becoming more complex and polygonal north-eastwards. (b) Simplified map outlining key structures and structural domains of the SPP and coloured accordingly to the timing of onset of growth, with blue indication earlier, Albian growth, and pink, Late Cretaceous. Seismic sections presented here in orange.

Figure 5: (a-c) NW-SE oriented lines showing a salt-cored fold belt above a landward-dipping base salt step and broadly thick salt on Domain I. The fold-belt present variable fold geometries but are predominantly cored by intra-salt shear zones (thick-black lines) and affected by outer-arc extension, with occasional reactive piercement on their core, which typically occurs where the base-salt becomes flat. Faults in black and pre-kinematic, tabular roof indicated by white ticks, which becomes progressively thicker landward showing the general younging direction of the foldbelt. (d) SW-NE oriented section over the salt walls and minibasins in the area with large salt evacuation at their centre due to a combination of extension and density-driven subsidence associated to ponding of mass-transport complexes (MTCs).

Figure 6: Seismic section of Domain II, with (a-b) WNW-ESE sections showing wide salt walls affected by intra-salt complex deformation and seaward-vergent shear zones and affected predominantly by inward-dipping and younging growth normal faults in their flanks and intercalated with RSBs and few salt-cored folds. The Albian interval is predominantly isopachous with only minor, local Albian growth of wall 3 in (a) and the bulk of supra-salt thickness variation occurring from Late Cretaceous-Paleocene within RSBs. (c) Same section of (b) with a pink polygon representing the salt interval with its base-salt static-corrected horizon showing the real base-salt geometry and the presence of a large landward-dipping ramp. (d) Section showing Late Cretaceous-Paleocene reactive salt walls that form along-strike, at the edge of the large salt walls 2 and 3 intercalated with Late-Cretaceous-Paleocene gentle salt-cored folds.(e) Section showing a similar reactive salt wall nucleating on the core of salt-cored fold formed by earlier contraction as indicated by the intra-salt shear zone.

Figure 7: Kinematic models showing evolution of walls of Domain II and landward-propagation of shortening and the foldbelt of Domain I by translation over a set of base-salt landward-dipping ramps over the Sugar Loaf High. In (a), model with initial salt relief due to an earlier Albian growth phase (Phase I) and, in (b), no earlier Albian growth (tabular Albian in green). As translation starts (Phase II) the system becomes temporarily pinned above the ramps and, due to initial thickness variations controlled by basal relief, the cross-sectional area of salt flowing onto the ramps is greater than the one flowing out; producing salt inflation and contraction. Continuous salt inflation and translation leads to progressive widening of the salt structure and development of RSBs over their basinward-flank above the base-salt flat where movement is faster; whereas their landward-flanks keep being uplifted and upturned. In the case of an earlier, Albian phase of growth (a), inflation results in piercement by active diapirism (Phase II), with eventual breakthrough and passive diapirism

(phase III). In the case of no previous growth (b), inflation results in development of a contractional anticline (Phases II-III). During Phases III-IV, differential translation and continuous thickening allow the velocity to build-up and the salt structure to eventually leave the ramp while extending over the base-salt high. In the case of an earlier passive diapir (a), extension is mostly cryptic and results in wide passive salt walls; whereas in the case of salt anticlines (b), a reactive diapir nucleates at their crests. As translation continues, contraction propagates landward and new salt-cored folds form as salt flow keeps being buttressed against the landward-dipping steps (Phase IV).

Figure 8: (a-b) NW-SE sections illustrating salt wall 5, which forms above narrow base-salt horst block at the edge of the Sugar-Loaf and is characterized by complex intra-salt deformation, intra-salt shear zone indicating early inflation, followed by extension and passive growth. The large width of the wall suggests part of the extension is cryptic, being accommodated by widening. This wall is limited downdip by a thick minibasins showing two thin RSBs sections that formed by translation above both base-salt ramps delimiting the pre-salt high. Further downdip, wall 6 occurs over another base-salt high and is characterized by a narrow reactive salt wall formed above a salt-cored fold to the north, at the edge of the base-salt high (a); and a wide salt wall with stronger evidence of contraction (intra-salt shearing and buckle-folding on its basinward-flank).In (c), the same section from (b) with a pink polygon representing the salt interval with its base-salt static-corrected horizon showing the real base-salt geometry and the presence of the base-salt horst beneath wall 5 and a landward-dipping ramp beneath wall 6.

Figure 9: (a) Complex base-salt geometries at the edge of the Sugar-Loaf High with ramps highlighted by grey polygons showing a NNE-oriented base-salt branch passing downdip to a NE-oriented landward-dipping ramp and further downdip to an ENE relay zone. (b) Kinematic model showing distribution of walls from Domains II and III, with marked shearing and rotation where base-salt topography abruptly changes, especially at the edge of the Sugar Loaf High. Structures to the south, over the Sugar Loaf High are oriented NNE, sub-parallel to the base-salt, curving progressively to the NE northwards. Structures further downdip, landward and over the ENE-oriented relay zone are also oriented sub-parallel to the ENE-NE structures, suggesting clockwise rotation and shearing relative to structures further south and/or landward. The wall over the NNE-oriented base-salt updip branch is sheared and rotated counter-clockwise as it reaches earlier a base-salt high, relative to its counterpart further south, over the Sugar Loaf High. The RSB formed immediately downdip of this NNE high translates and rotates clockwise and the wall further downdip over the NE-oriented base-salt high is sheared clockwise as its northern edge is able to move faster while its southern part is being buttressed against the edge of the Sugar-Loaf; producing a sigmoidal plan-view geometry.

Figure 10 (a-b): Physical models simulating gravity-driven salt-detached translation around three discontinuous pre-salt tilted blocks and the effects of base-salt relief on salt flow with pre-salt blocks highlighted in white boxes (adapted from Dooley et al., 2018). (a) Overhead views showing rotation up to 67° at the edge of the pre-salt blocks. (b) Dip-parallel displacement and Y motions (N-S movements) of relative of same time-steps of (a) showing divergent flow around the updip edges of pre-salt block and convergent flow around their downdip edges. For full model design and material details, see Dooley et al. (2017).

Figure 11: (a-b) NW-SE oriented sections of Domain IV showing tall salt walls (7-9) and with abrupt flank upturns and thick, welded minibasins with abrupt cutoffs and onlaps against the walls and turtle or bowl geometries, and raised rims. These aspects indicate they formed primarily by density-driven subsidence and passive diapirism over a broadly flat base-salt topography. Walls further downdip become more affected by normal faults, denoting progressively earlier effects of regional stresses, mainly associated with extension. (c) NW-SE narrow reactive salt walls formed at the south edge of Domain IV, near Domain III. (d)

Wider NW-SE reactive salt wall further north, showing signs of earlier density-driven growth, a large turtle anticline formed above a set of Albian narrow and abrupt anticlines.

Figure 12: Dip-oriented sections illustrating salt-related structural styles and associated RSBs over the Tupi High and smaller pre-salt tilted blocks further downdip in Domain V. (a-b) Regional sections showing contraction (buckle-folds) over the landward-dipping edge of the Tupi High, passing downdip to extended folds and reactive diapirs over the broadly flat base-salt segment downdip, subsidence and development of RSBs above the large basinward-dipping base salt and a contractional fold-thrust belt further downdip. (b) Same section with representation of real base-salt geometry with a salt polygon with the static-corrected base-salt horizon. (c) Close-up of updip salt-cored buckle folds formed by buttressing against the crest of the Tupi High, monoclinal geometry overlain by a RSB over the large base-salt basinward-dipping ramp and additional contraction immediately downdip of it, with stacking of intra-salt reverse shear zones, buckle-folding and thickening of the salt interval. (d) Section showing minor updip extension and reactive rise at the crest of an earlier contractional structure at the crest of the Tupi, passing downdip to an open fold and RSB above its basinward-dipping ramp and further downdip to a fold-thrust belt associated with RSBs and squeezed diapirs, fold injection and thrust piercement indicating renewed pulses of contraction as translation occurred over series of smaller pre-salt highs.(e) Section showing similar features downdip of the Tupi High and along-strike variation of a squeezed diapir from (d) to back-thrust-piercement of salt. (f) Section showing stacking of reverse basinward-vergent intra-salt shear zones and consequent thickening of the salt interval with active piercement and disruption of the foldbelt roof behind the large pre-salt high downdip of the largest Tupi High.

Figure 13: (a) Kinematic model showing the cross-sectional evolution of Domain V by translation over the Tupi High and closely-spaced pre-salt tilted blocks downdip. Translation over the gentle landward-dipping step of the Tupi results in partial pinning of the system against the crest of the Tupi High and development of a foldbelt updip. Translation over the Tupi High basinward-dipping edge results in salt subsidence, development of RSBs above it and contraction further downdip as movement is buttressed by a series of smaller base-salt steps, in which RSBs also form over their basinward-dipping side. Mild extension occurs at the crest of the Tupi High, resulting in minor faulting and unfolding of earlier folds formed updip. Extension is, however, overprinted by contraction as the system moves downdip over the set of smaller base-salt highs where renewed pulses of contraction resulting in fold-injection, squeezing and thrust piercement. (b) Map-view kinematic model illustrating radial flow around smaller, broadly rectangular pre-salt blocks; which results in divergence around it and convergence and pinning behind it. This produces coalescence and thickening of salt-cored and development of NW-oriented ridges folds behind smaller pre-salt highs.

Figure 14: NW-SE sections of Domain VI: (a) Section to the south, over the NNW branch of the Tupi High showing reactive salt walls over the base-salt horst block passing to a salt-cored contractional foldbelt downdip of the base-salt high, all being associated with Late Cretaceous-Paleocene RSBs. The largest walls show an earlier, Albian phase of growth, with significant thickness variations and top-Albian unconformities. (b) Section to the north, farther of the Tupi High, showing similar style of deformation with a broader reactive diapir updip and a gentler foldbelt associated with RSBs further downdip, but with relatively stronger influence of density-driven processes as seen by intermediate nearly welded, broadly symmetric minibasins and a salt wall driven by halokinetic active diapirism.

Figure 15: (a) Location map adapted from Guerra and Underhill (2012) showing the curvature of the margin and the associated Cretaceous hinge line. Their study-area in black and ours in white polygons with their equivalent regional, 2D based top-salt structure map in (b); and combination of our top-salt structure map with their 3D-based top-salt structure map located immediately to the north of our study-area. In (d) a simplified diagram combining the two maps and showing the presence of W-E to NW-SE extensional ridges north of our study-

area, passing southwards to contractional ridges and anticlines that diverge around the Tupi High, with few structures moving over the high and being reactivated as extensional walls.

Figure 16: Idealized viscous shear drag (i.e. Couette flow) model showing salt streamlines (black line) and flux variations across base-salt relief that resulted in the observed deformational style in the SPP. Salt inflation and contraction over base-salt landward-dipping ramps and subsidence with updip extension and downdip contraction over base-salt basinward-dipping ramps. (b)-(c) Physical models simulating salt-detached translation of a mechanically-layered salt with (a) negligible roof and (b) thick roof showing a first-order Couette flow profile and more variable second-order flow; both of which evolve through time and become more complex and affected by Poiseuille flow as the overburden thickens (adapted from Weijermars et al., 2014). Viscous silicone polymer (black) alternates with frictional-plastic dry sand (thin, coloured layers, each 1 mm thick). For full model details, see Cartwright et al. (2012).

Figure 17: Kinematic model explaining the origin of the Albian Gap by 30 km of Albian extension and additional 30 km of extension with coeval salt expulsion during the Late Cretaceous-Paleocene.

Figures

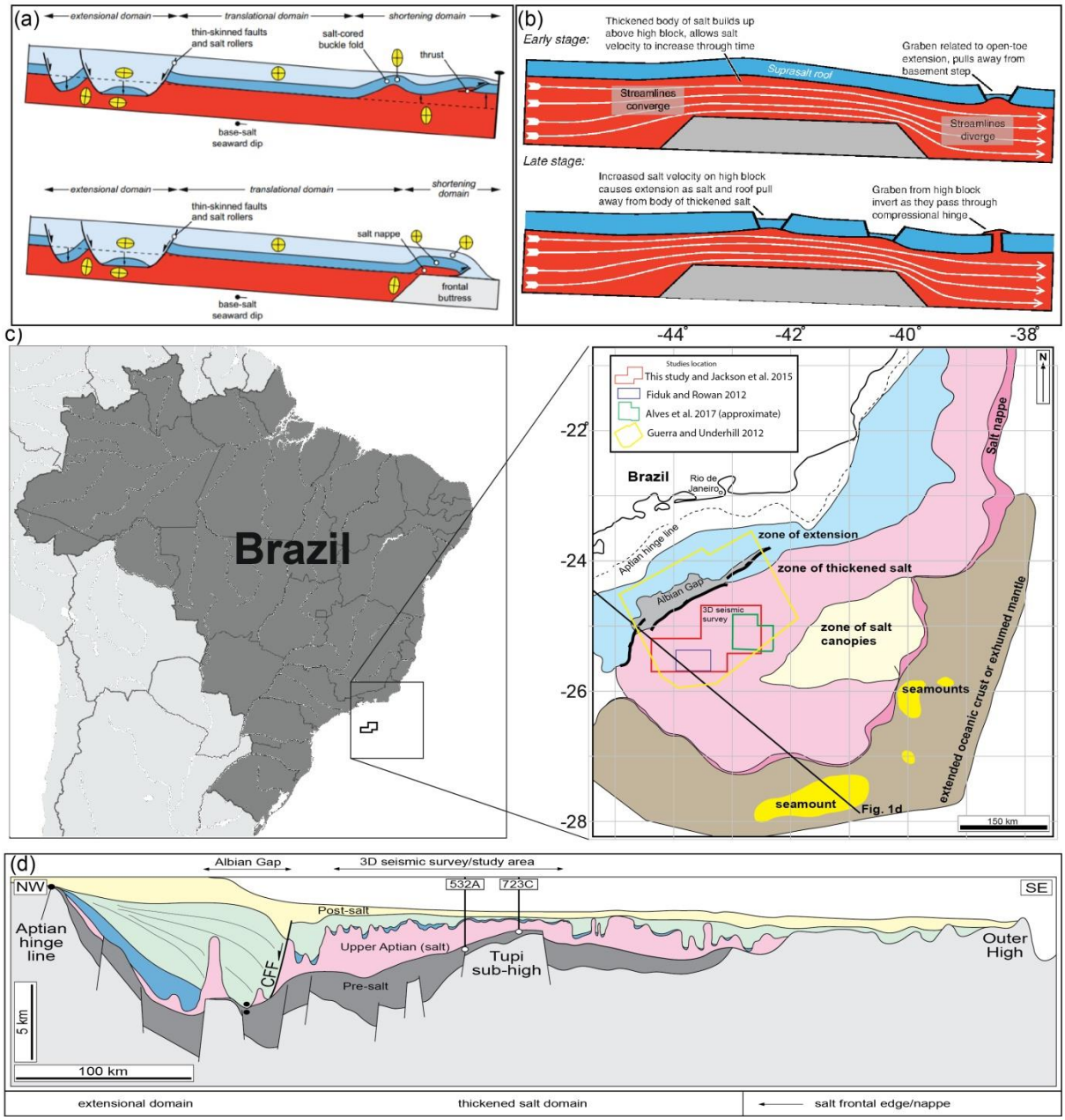

Figure 1

Figure 2

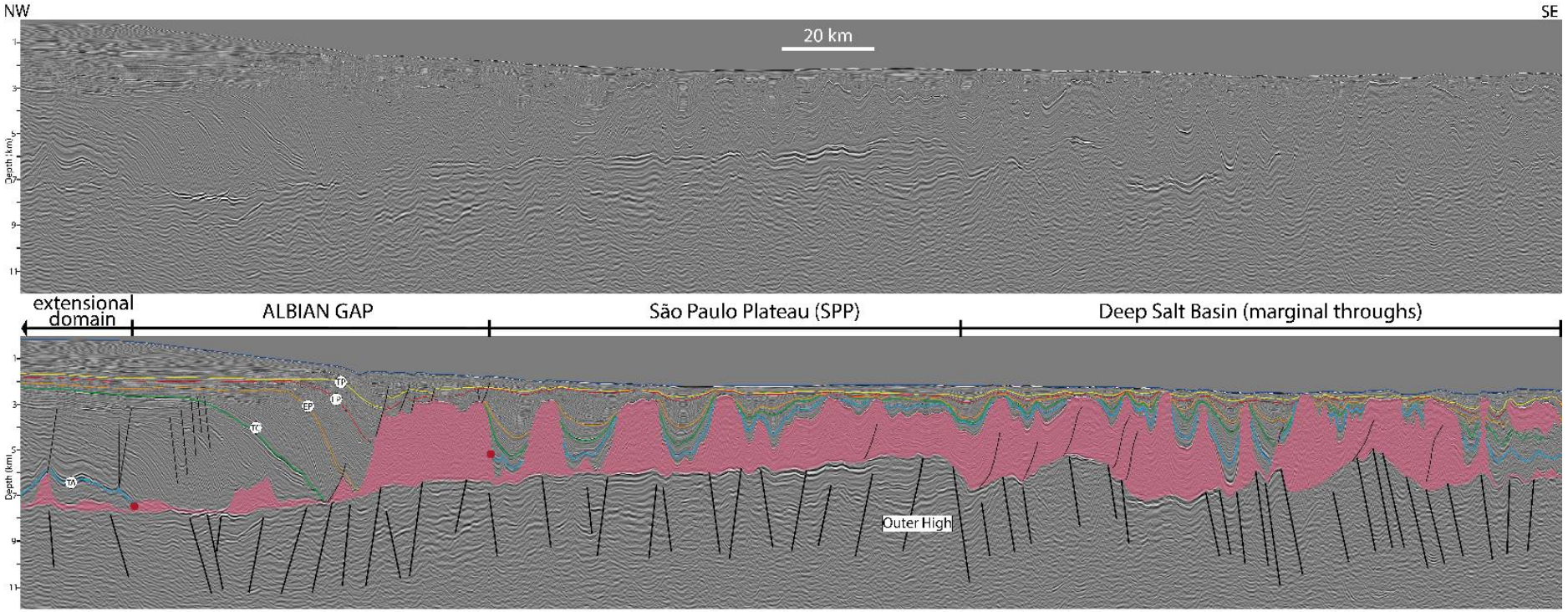
NW
SE
20 km
Depth (km)
extensional domain
ALBIAN GAP
São Paulo Plateau (SPP)
Deep Salt Basin (marginal throughs)
TA
TK
EP
LP
TP
Outer High

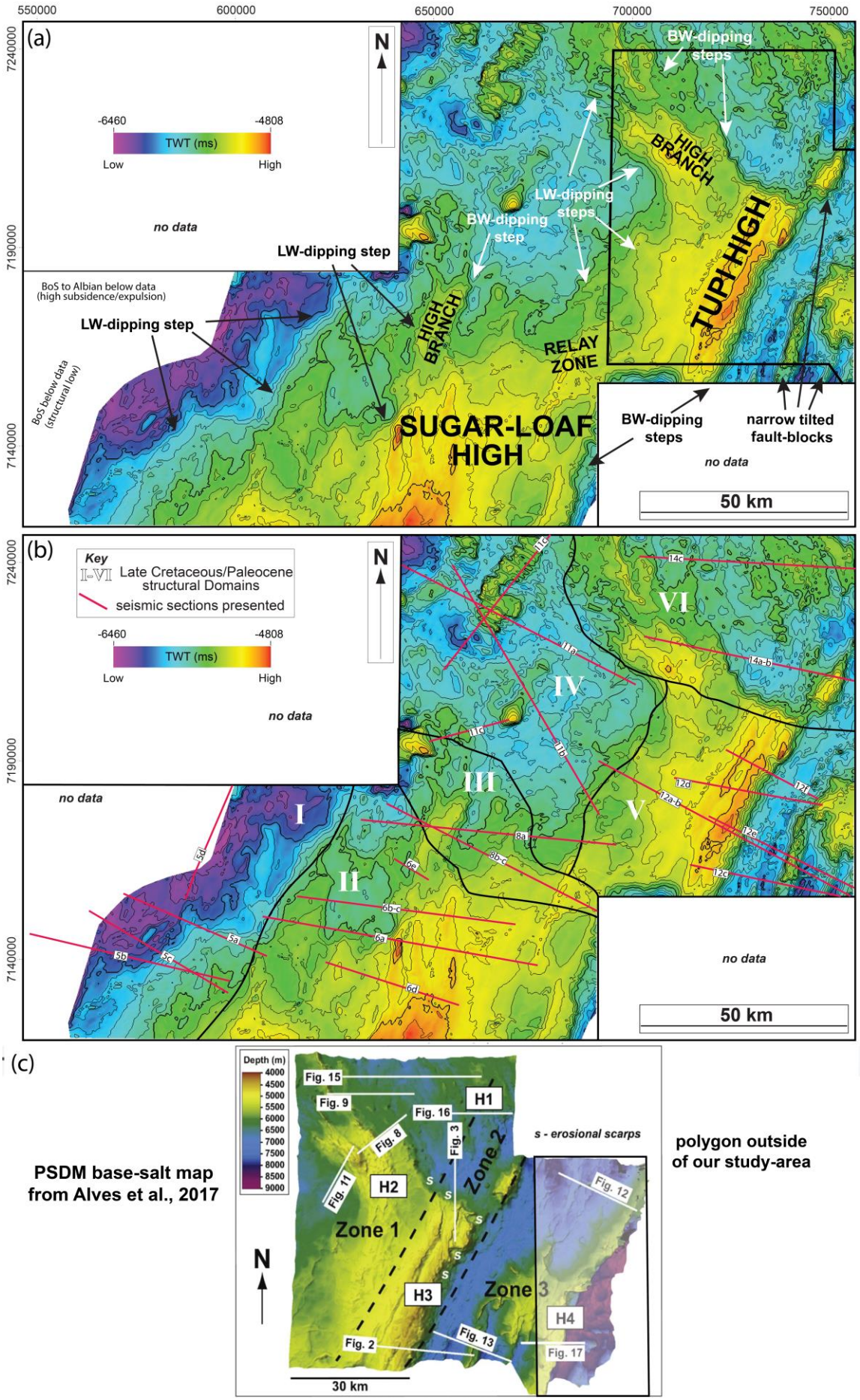
550000
600000
650000
700000
750000
7240000
7190000
7140000
(a)
N
-6460
-4808
TWT (ms)
Low
High
no data
BW-dipping steps
HIGH BRANCH
LW-dipping steps
BW-dipping step
LW-dipping step
TUPI HIGH
BoS to Albian below data (high subsidence/expulsion)
LW-dipping step
HIGH BRANCH
RELAY ZONE
BoS below data (structural low)
SUGAR-LOAF HIGH
BW-dipping steps
narrow tilted fault-blocks
no data
50 km
(b)
Key
I-VII Late Cretaceous/Paleocene structural Domains
seismic sections presented
-6460
-4808
TWT (ms)
Low
High
no data
N
VI
IV
III
V
I
II
no data
no data
50 km
(c)
Depth (m)
4000
4500
5000
5500
6000
6500
7000
7500
8000
8500
9000
Fig. 15
Fig. 9
Fig. 16
H1
Fig. 8
Fig. 3
s - erosional scarps
Fig. 11
H2
Zone 2
Zone 1
Fig. 12
N
H3
Zone 3
H4
Fig. 2
Fig. 13
Fig. 17
30 km
PSDM base-salt map from Alves et al., 2017
polygon outside of our study-area

Figure 3

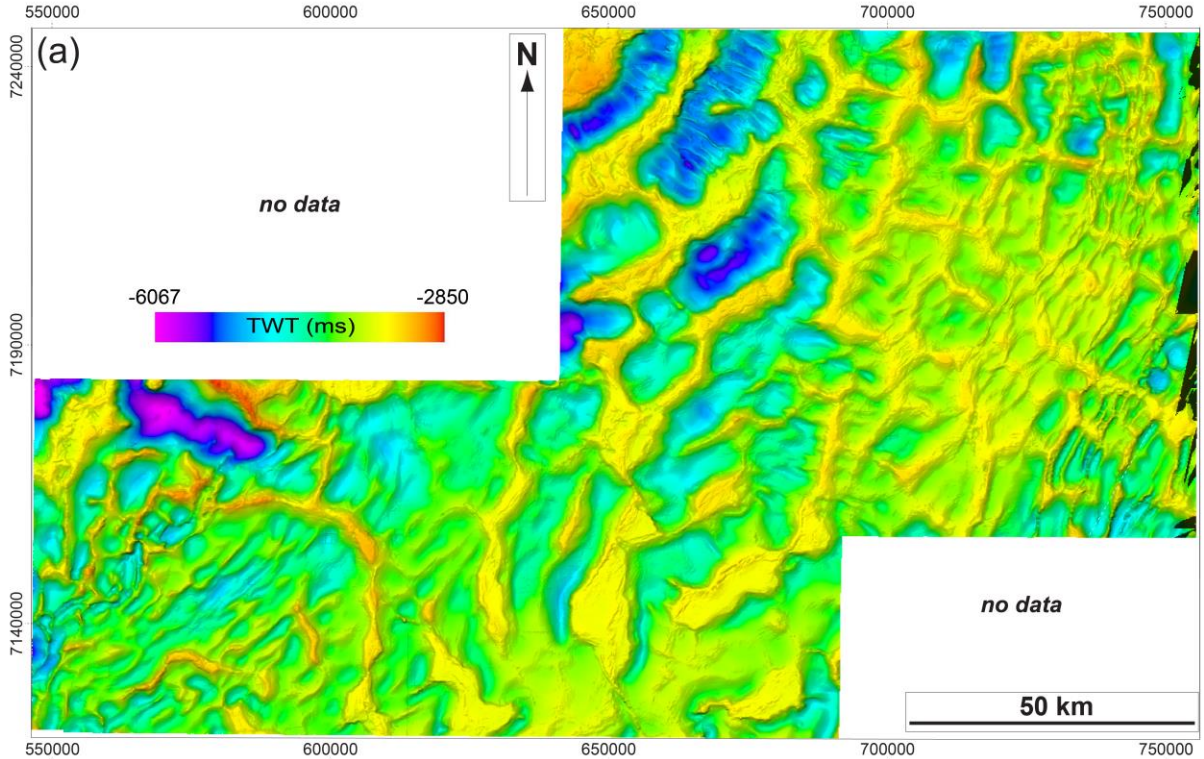

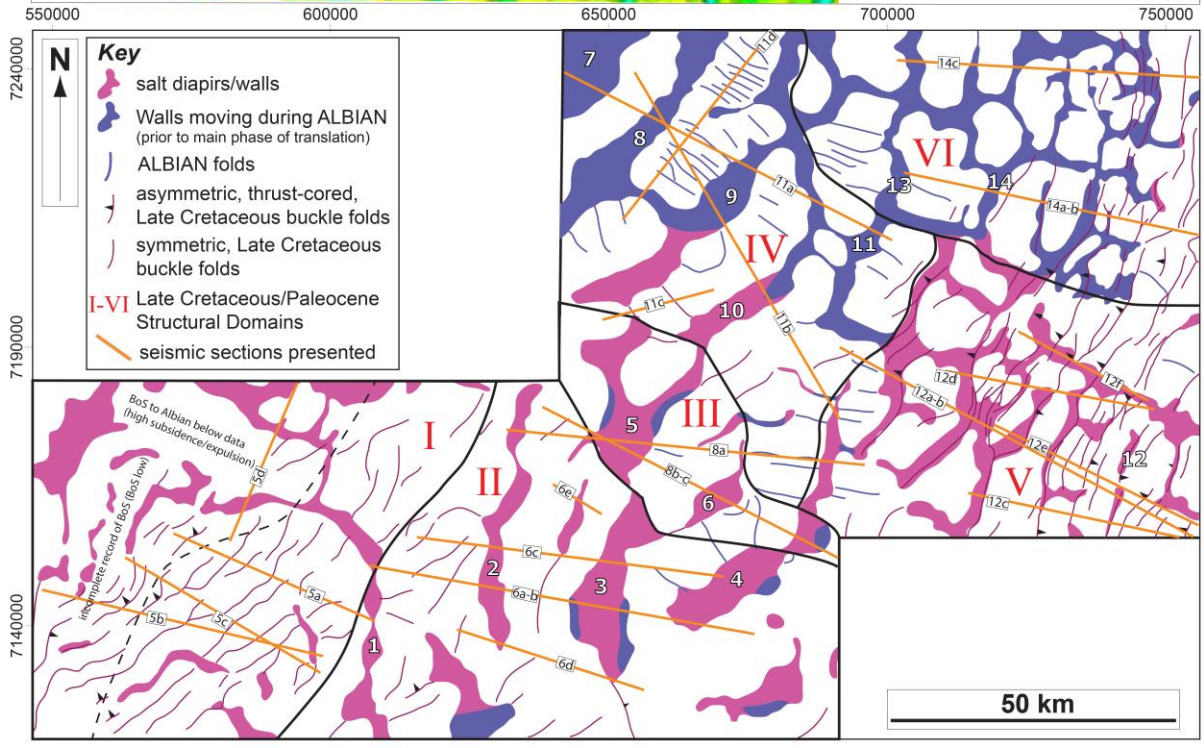

Figure 4

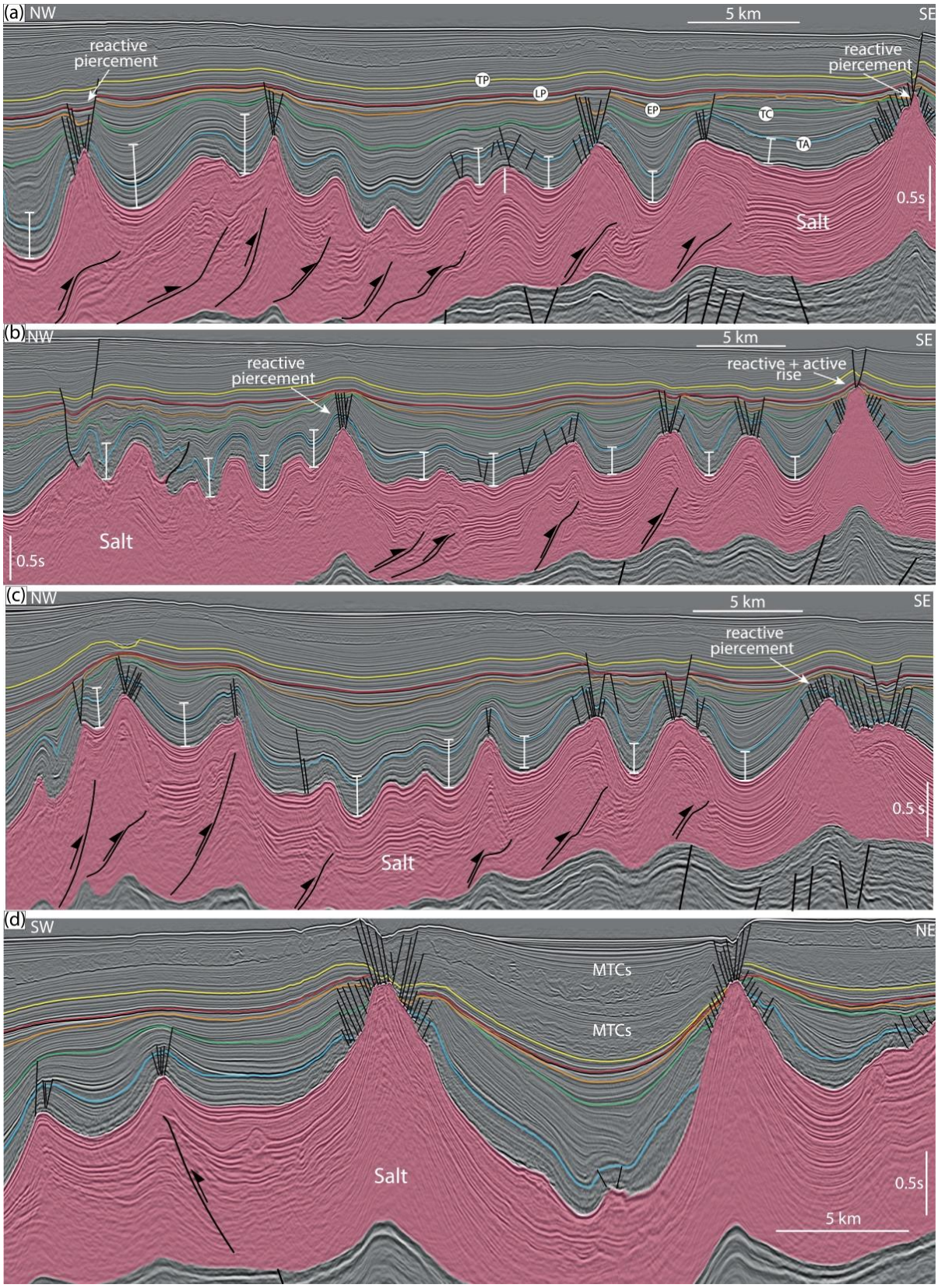
(a) NW
5 km
SE
reactive piercement
reactive piercement
TP
LP
EP
TC
TA
0.5s
Salt
(b) NW
5 km
SE
reactive piercement
reactive + active rise
Salt
0.5s
(c) NW
5 km
SE
reactive piercement
0.5 s
Salt
(d) SW
NE
MTCs
MTCs
Salt
0.5s
5 km

Figure 5

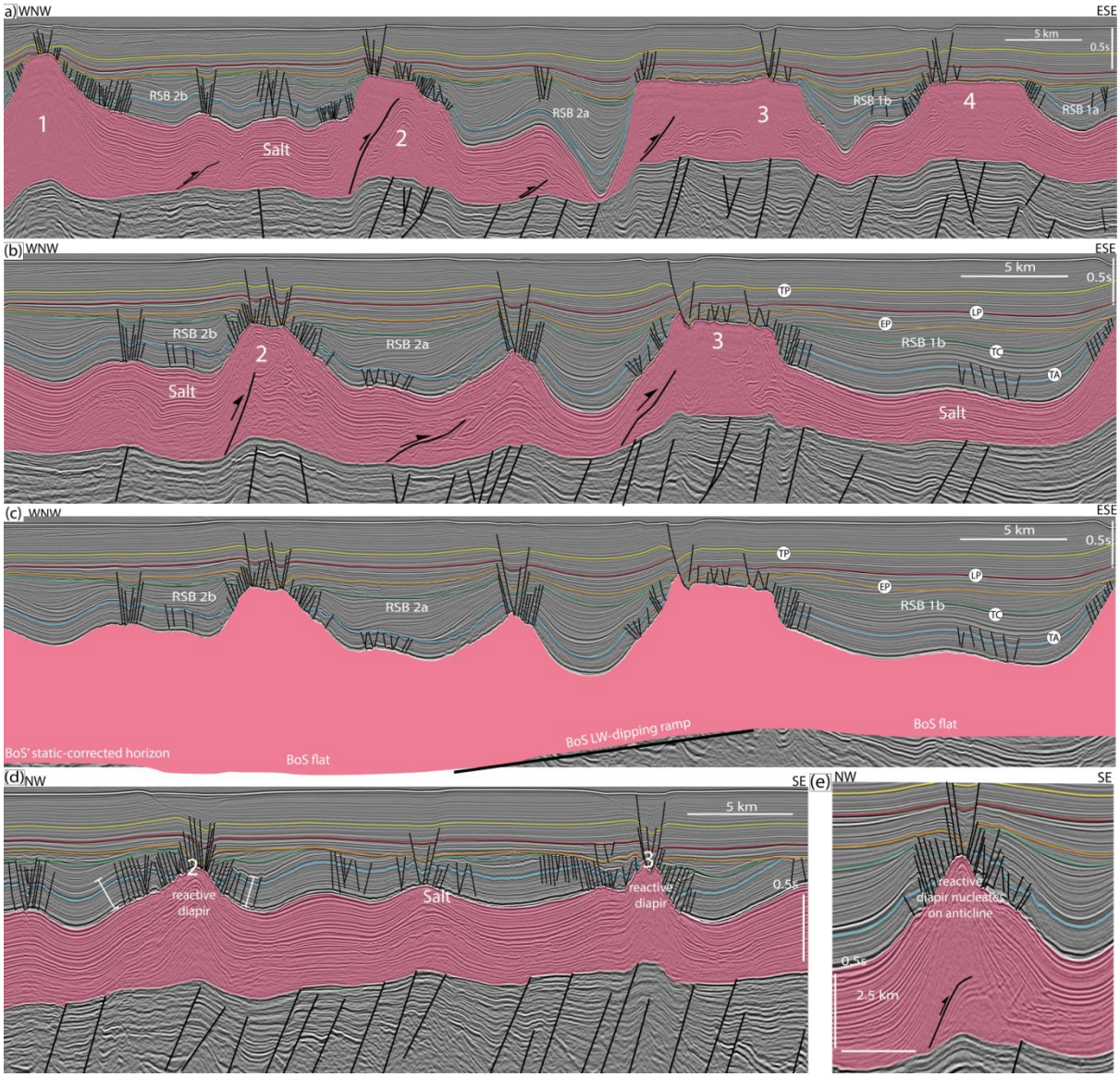
a) WNW
ESE
5 km
0.5s
RSB 2b
RSB 2a
RSB 1b
RSB 1a
1
2
3
4
Salt
(b) WNW
ESE
5 km
0.5s
RSB 2b
RSB 2a
RSB 1b
TP
EP
LP
TC
TA
2
3
Salt
Salt
(c) WNW
ESE
5 km
0.5s
RSB 2b
RSB 2a
RSB 1b
TP
EP
LP
TC
TA
BoS' static-corrected horizon
BoS flat
BoS LW-dipping ramp
BoS flat
(d) NW
SE
5 km
0.5s
2
reactive diapir
Salt
3
reactive diapir
(e) NW
SE
reactive diapir nucleated on anticline
0.5s
2.5 km

Figure 6

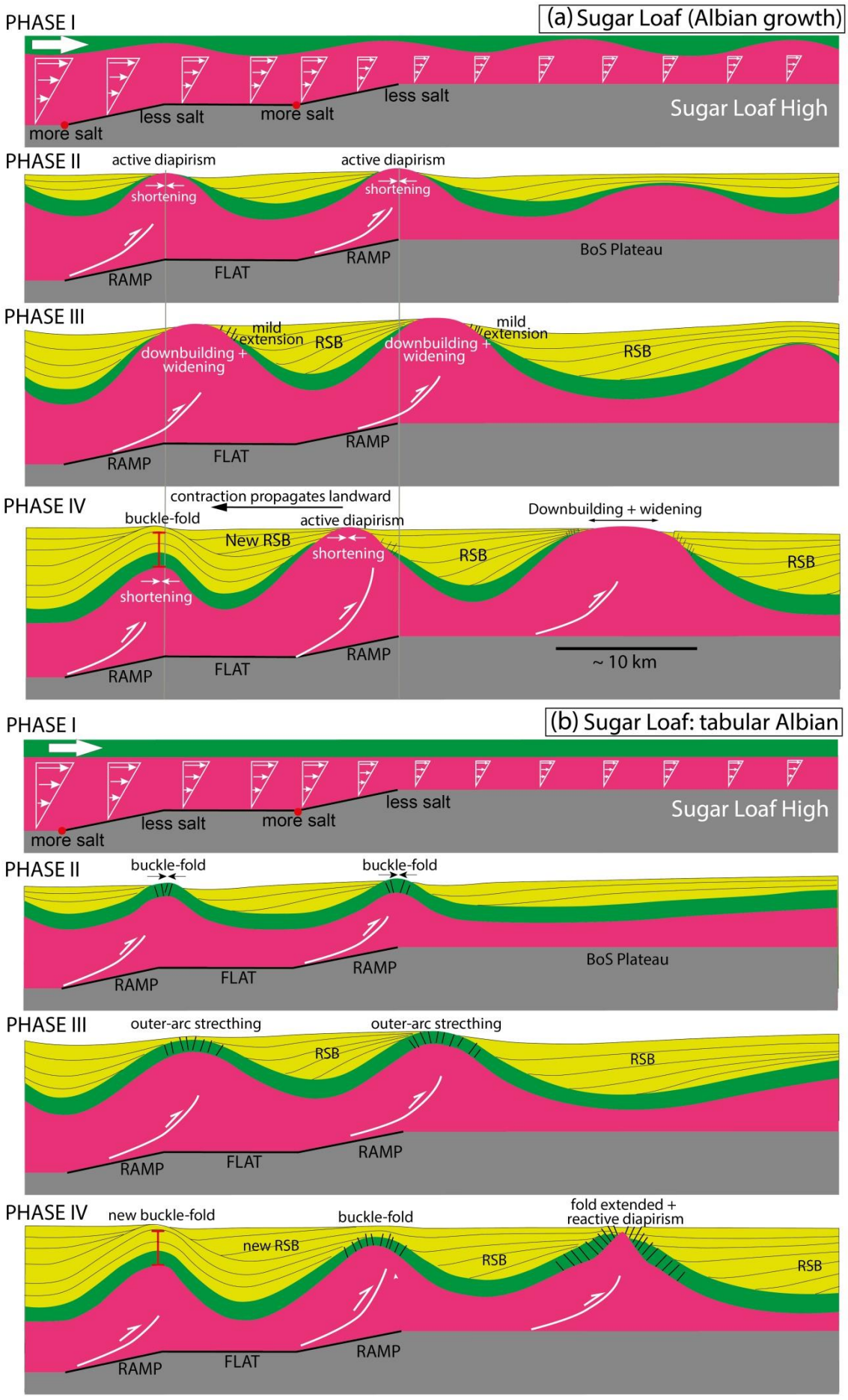
(a) Sugar Loaf (Albian growth)
PHASE I
less salt
more salt
less salt
more salt
Sugar Loaf High
PHASE II
active diapirism
active diapirism
shortening
shortening
RAMP
FLAT
RAMP
BoS Plateau
PHASE III
mild extension
RSB
downbuilding + widening
mild extension
downbuilding + widening
RSB
RAMP
FLAT
RAMP
PHASE IV
contraction propagates landward
buckle-fold
active diapirism
Downbuilding + widening
New RSB
shortening
RSB
RSB
shortening
RAMP
FLAT
RAMP
~ 10 km
(b) Sugar Loaf: tabular Albian
PHASE I
less salt
more salt
less salt
more salt
Sugar Loaf High
PHASE II
buckle-fold
buckle-fold
RAMP
FLAT
RAMP
BoS Plateau
PHASE III
outer-arc strecthing
outer-arc strecthing
RSB
RSB
RAMP
FLAT
RAMP
PHASE IV
new buckle-fold
buckle-fold
fold extended + reactive diapirism
new RSB
RSB
RSB
RAMP
FLAT
RAMP

Figure 7

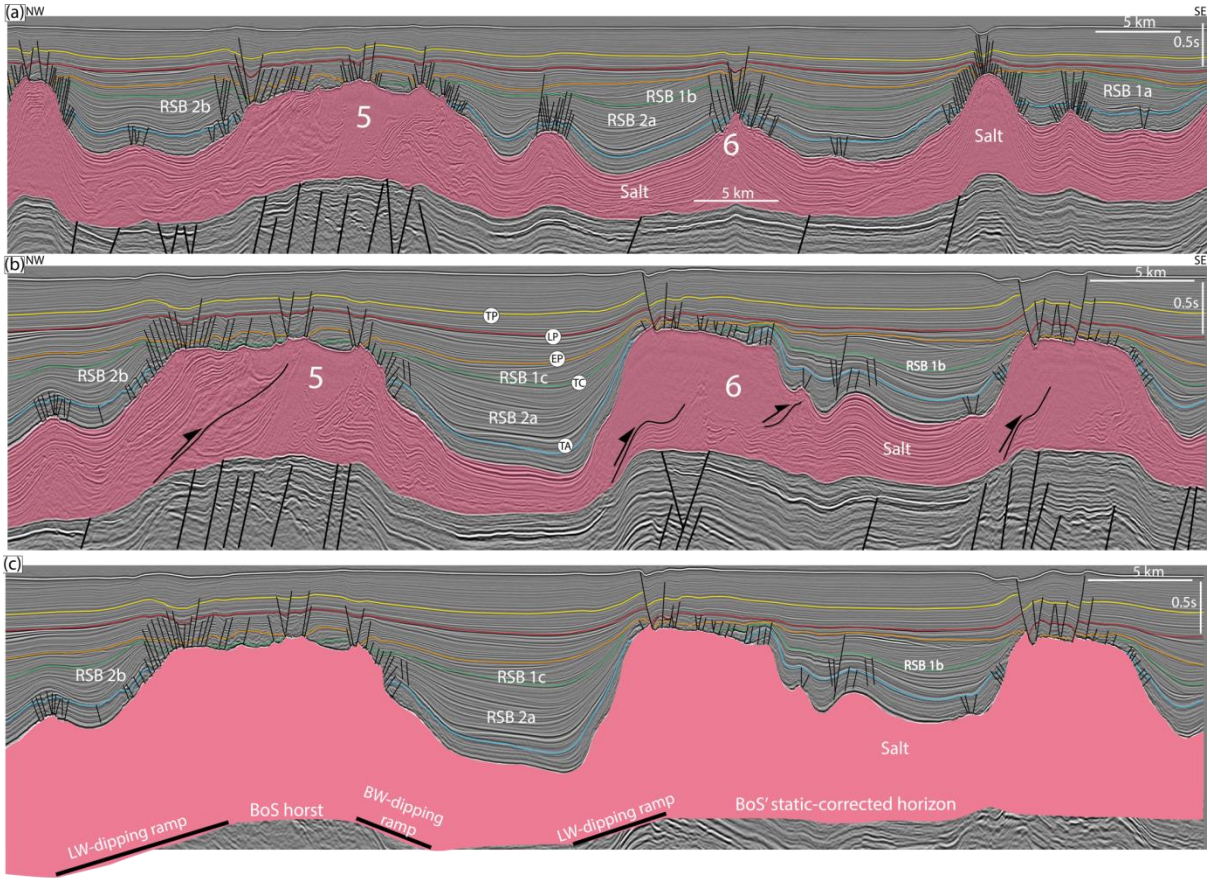

Figure 8

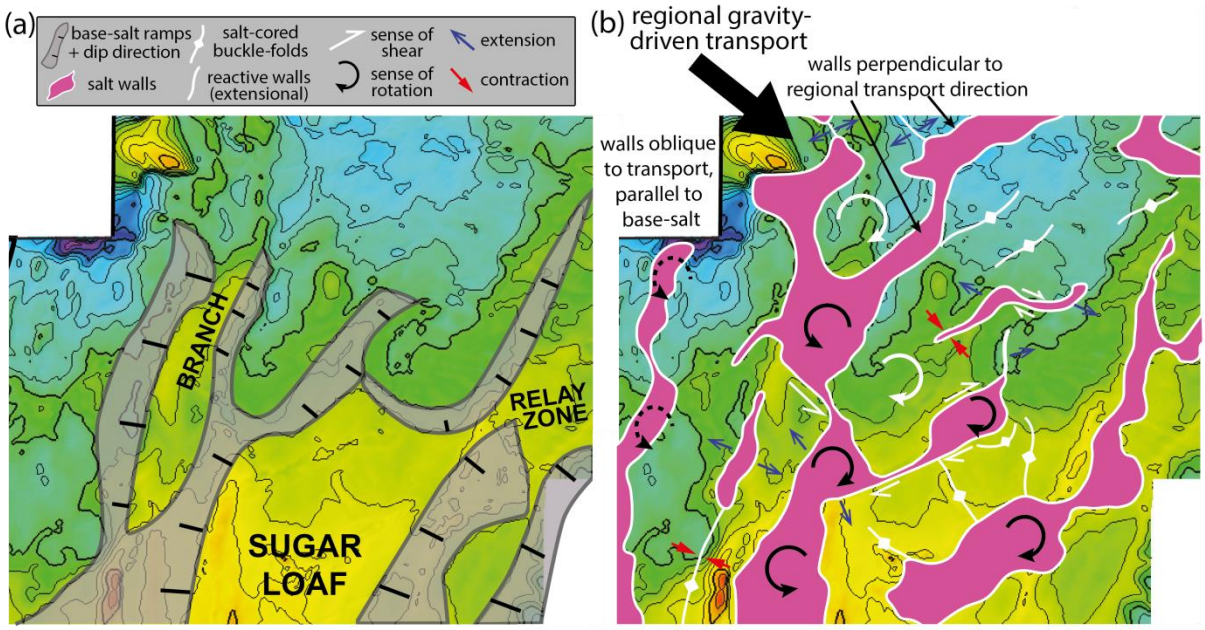
(a)
base-salt ramps + dip direction
salt-cored buckle-folds
sense of shear
extension
salt walls
reactive walls (extensional)
sense of rotation
contraction
BRANCH
RELAY ZONE
SUGAR LOAF
(b) regional gravity-driven transport
walls perpendicular to regional transport direction
walls oblique to transport, parallel to base-salt

Figure 9

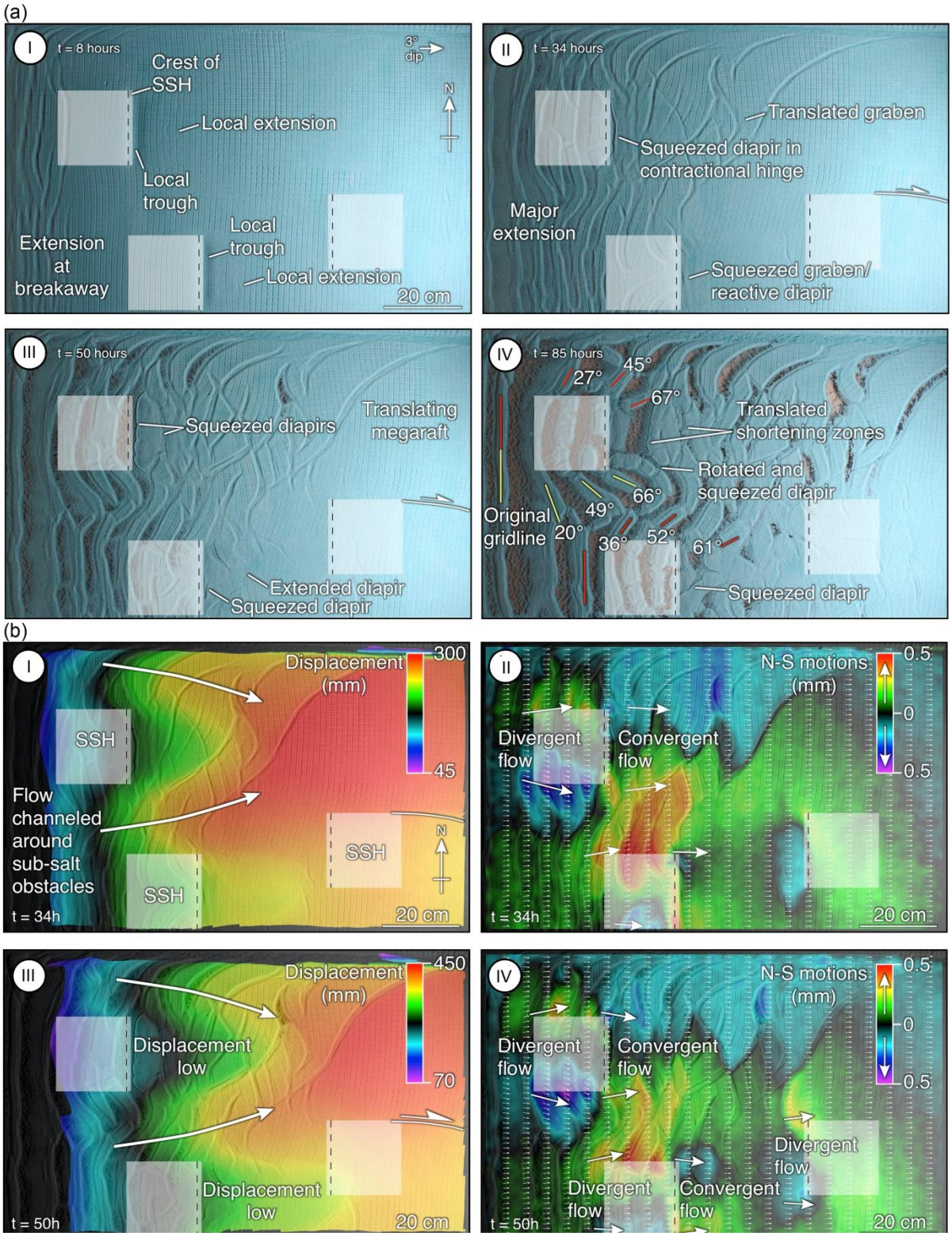
(a)
I
t = 8 hours
3° dip
Crest of SSH
Local extension
Local trough
Extension at breakaway
Local trough
Local extension
N
20 cm
II
t = 34 hours
Translated graben
Squeezed diapir in contractional hinge
Major extension
Squeezed graben/ reactive diapir
III
t = 50 hours
Squeezed diapirs
Translating megaraft
Extended diapir
Squeezed diapir
IV
t = 85 hours
27°
45°
67°
Translated shortening zones
Rotated and squeezed diapir
66°
49°
Original gridline
20°
36°
52°
61°
Squeezed diapir
(b)
I
Displacement (mm)
300
45
SSH
Flow channeled around sub-salt obstacles
SSH
SSH
N
t = 34h
20 cm
II
N-S motions (mm)
0.5
0
0.5
Divergent flow
Convergent flow
t = 34h
20 cm
III
Displacement (mm)
450
70
Displacement low
Displacement low
t = 50h
20 cm
IV
N-S motions (mm)
0.5
0
0.5
Divergent flow
Convergent flow
Divergent flow
Divergent flow
Convergent flow
t = 50h
20 cm

Figure 10

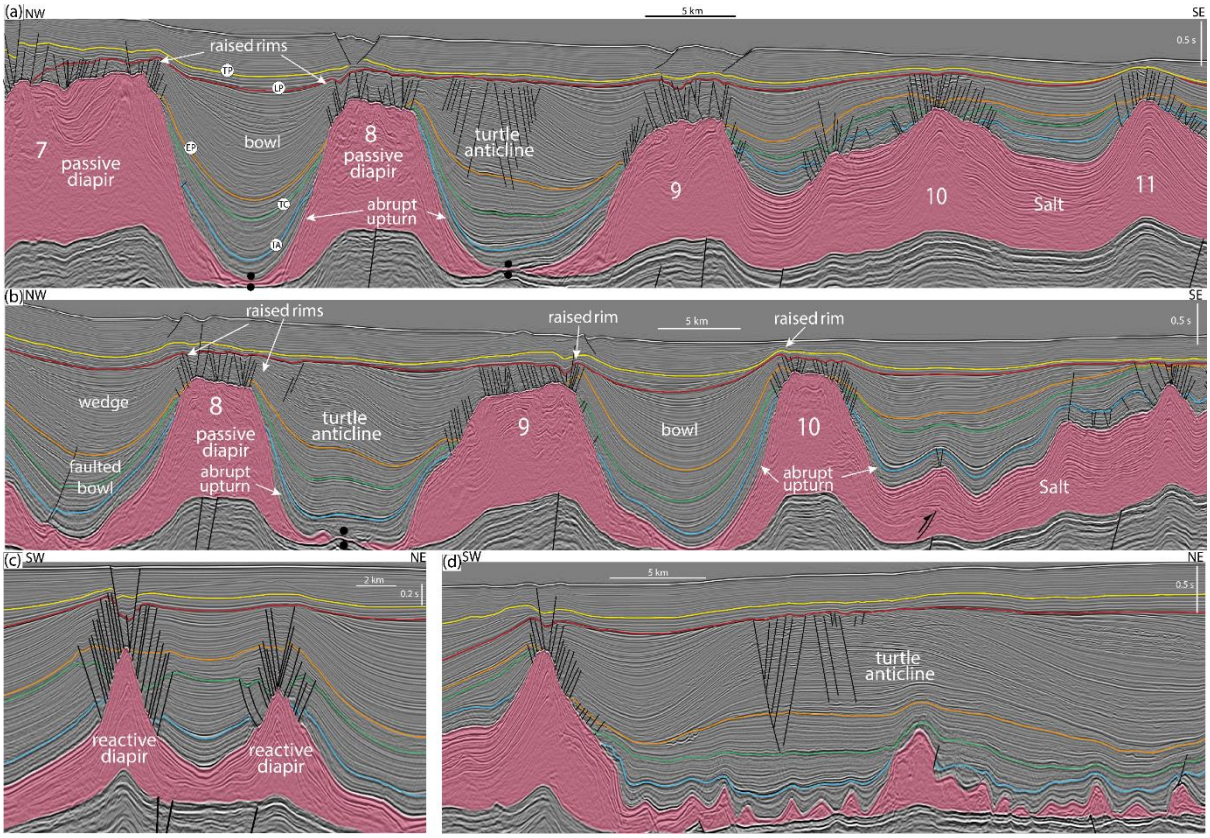
(a) NW
SE
5 km
0.5 s
raised rims
TP
LP
EP
TC
LA
7
passive diapir
bowl
8
passive diapir
turtle anticline
abrupt upturn
9
10
Salt
11
(b) NW
SE
raised rims
raised rim
5 km
raised rim
0.5 s
wedge
faulted bowl
8
passive diapir
abrupt upturn
turtle anticline
9
bowl
10
abrupt upturn
Salt
(c) SW
NE
2 km
0.2 s
reactive diapir
reactive diapir
(d) SW
NE
5 km
0.5 s
turtle anticline

Figure 11

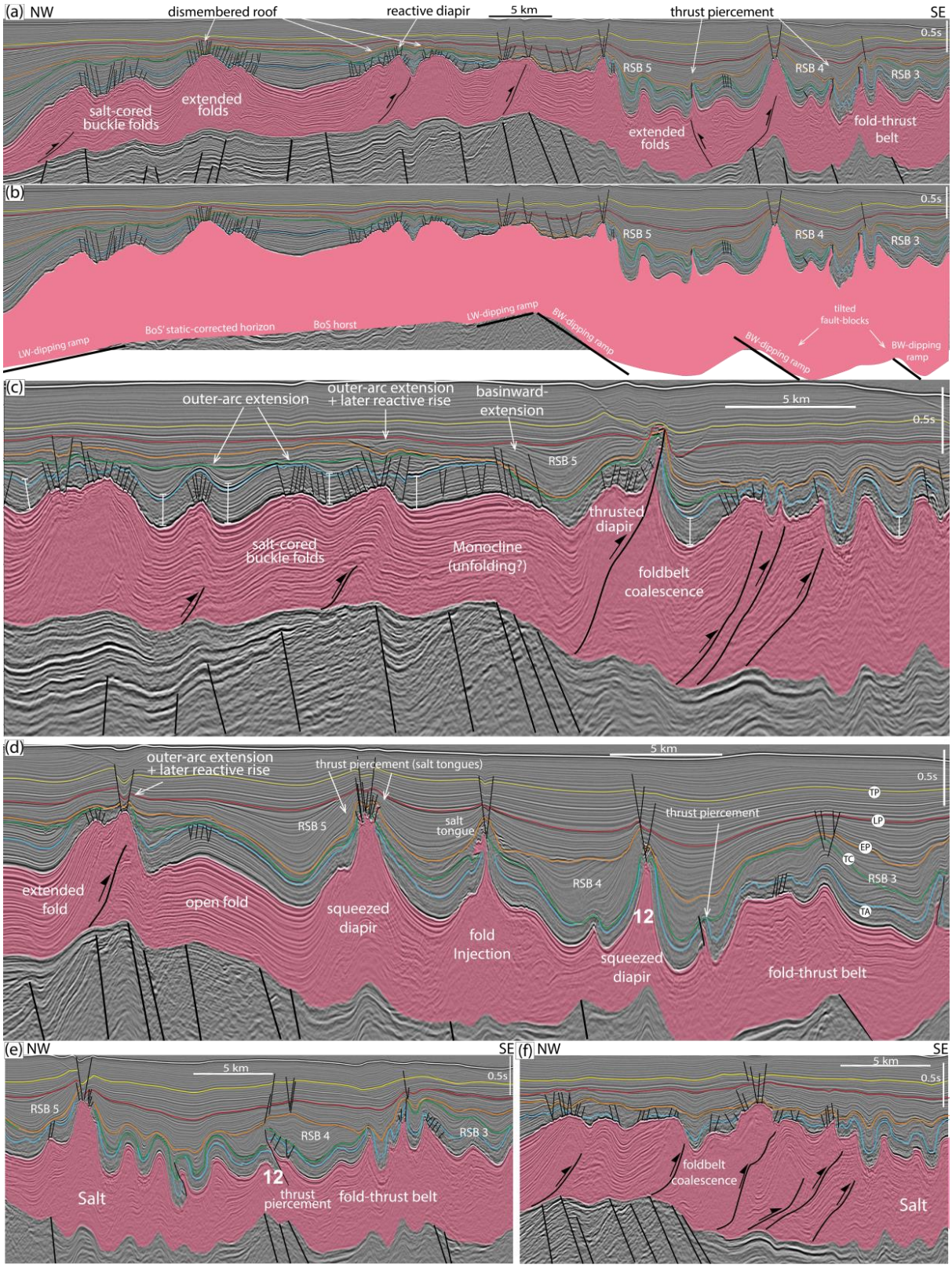
(a) NW
dismembered roof
reactive diapir
5 km
thrust piercement
SE
0.5s
salt-cored buckle folds
extended folds
RSB 5
RSB 4
RSB 3
extended folds
fold-thrust belt
(b)
0.5s
RSB 5
RSB 4
RSB 3
LW-dipping ramp
BoS' static-corrected horizon
BoS horst
LW-dipping ramp
BW-dipping ramp
tilted fault-blocks
BW-dipping ramp
BW-dipping ramp
(c)
outer-arc extension
outer-arc extension + later reactive rise
basinward-extension
5 km
0.5s
RSB 5
thrusted diapir
salt-cored buckle folds
Monocline (unfolding?)
foldbelt coalescence
(d)
5 km
outer-arc extension + later reactive rise
thrust piercement (salt tongues)
0.5s
TP
LP
FP
TC
TA
RSB 5
salt tongue
thrust piercement
RSB 3
RSB 4
extended fold
open fold
squeezed diapir
12
fold Injection
squeezed diapir
fold-thrust belt
(e) NW
SE
5 km
0.5s
RSB 5
RSB 4
RSB 3
12
Salt
thrust piercement
fold-thrust belt
(f) NW
SE
5 km
0.5s
foldbelt coalescence
Salt

Figure 12

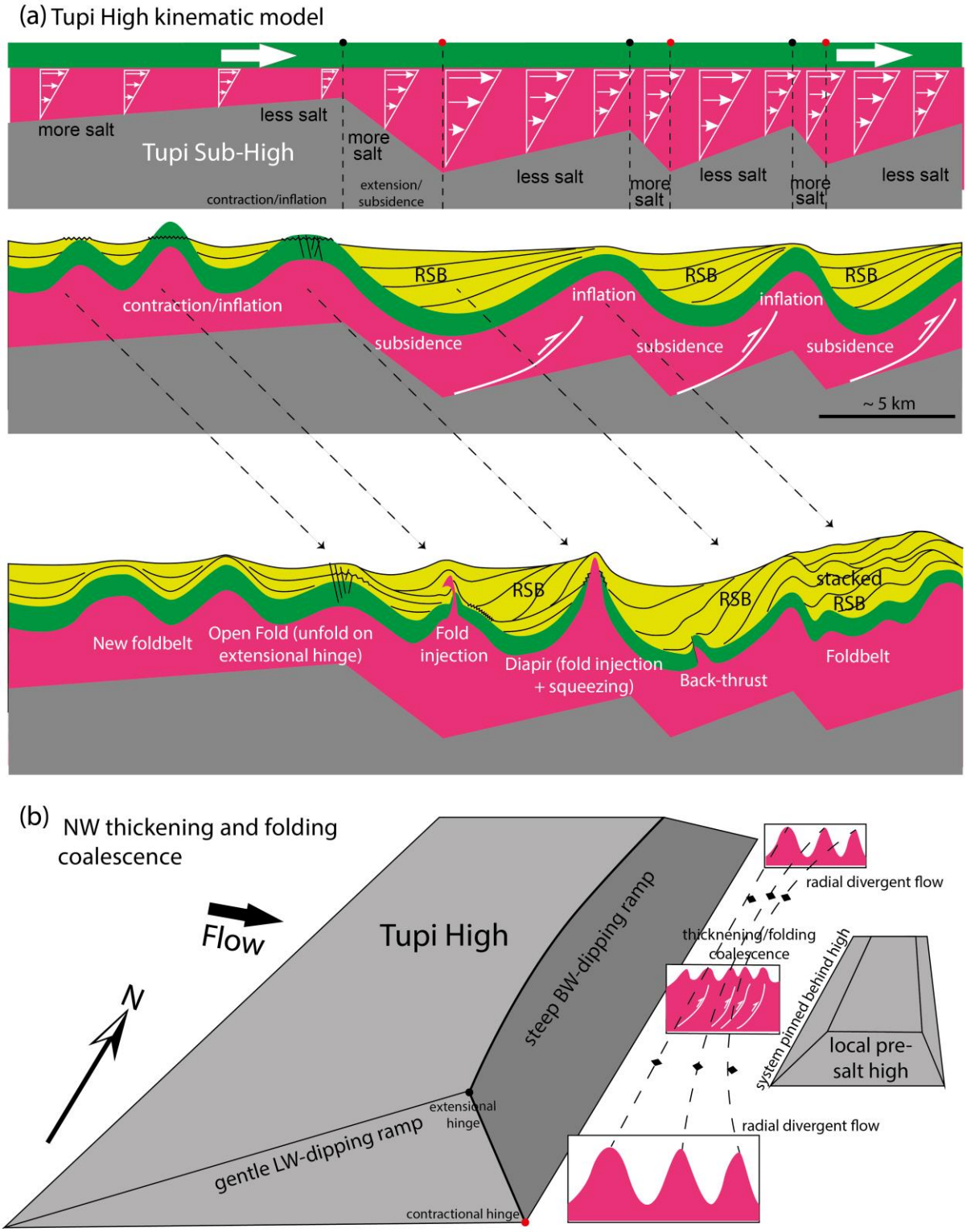
(a) Tupi High kinematic model
more salt
less salt
more salt
Tupi Sub-High
contraction/inflation
extension/ subsidence
less salt
more salt
less salt
more salt
less salt
RSB
RSB
RSB
contraction/inflation
inflation
inflation
subsidence
subsidence
subsidence
~ 5 km
stacked RSB
RSB
RSB
New foldbelt
Open Fold (unfold on extensional hinge)
Fold injection
Diapir (fold injection + squeezing)
Back-thrust
Foldbelt
(b) NW thickening and folding coalescence
Flow
N
Tupi High
steep BW-dipping ramp
radial divergent flow
thickening/folding coalescence
system pinned behind high
local pre-salt high
radial divergent flow
extensional hinge
gentle LW-dipping ramp
contractional hinge

Figure 13

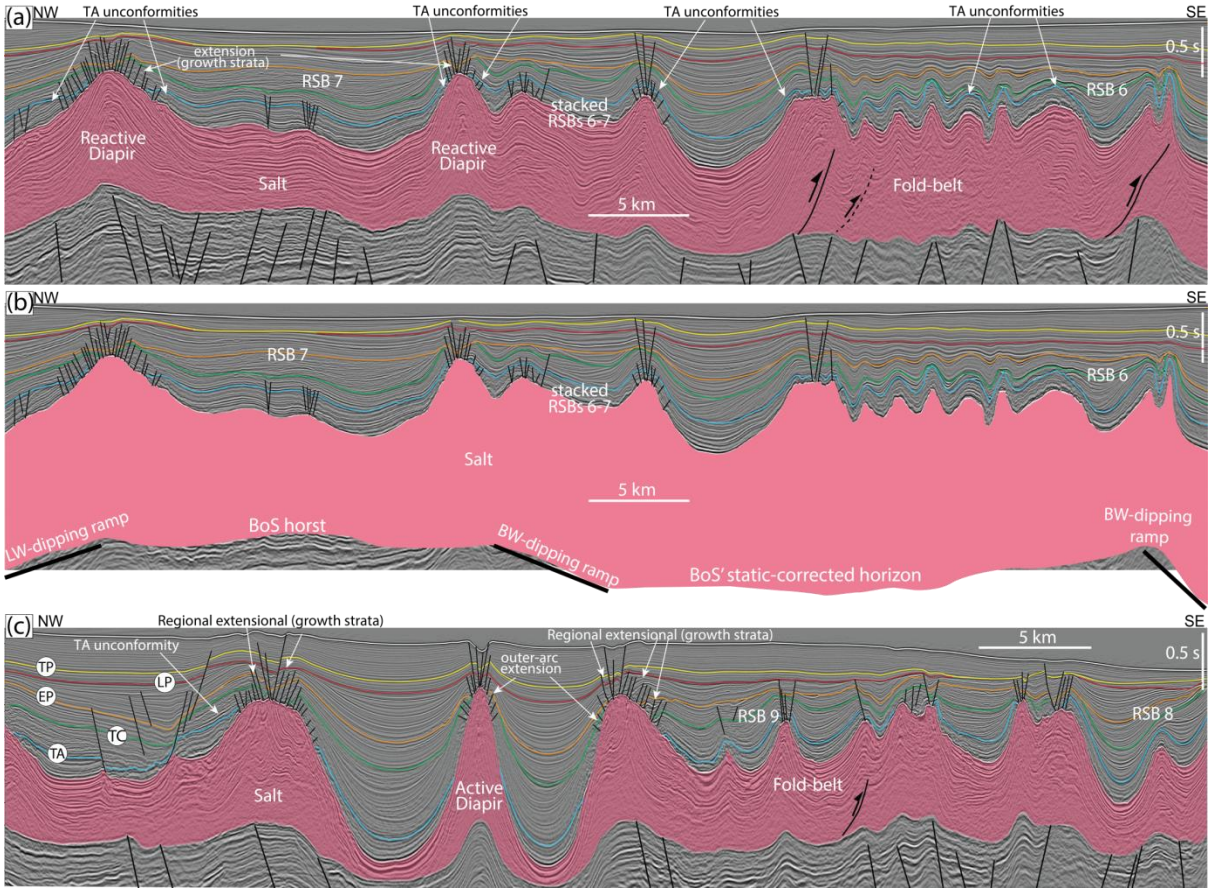
(a)
NW
TA unconformities
TA unconformities
TA unconformities
TA unconformities
SE
extension (growth strata)
RSB 7
stacked RSBs 6-7
RSB 6
0.5 s
Reactive Diapir
Reactive Diapir
Salt
5 km
Fold-belt
(b)
NW
SE
RSB 7
stacked RSBs 6-7
RSB 6
0.5 s
Salt
5 km
LW-dipping ramp
BoS horst
BW-dipping ramp
BW-dipping ramp
BoS' static-corrected horizon
(c)
NW
Regional extensional (growth strata)
Regional extensional (growth strata)
SE
TA unconformity
outer-arc extension
5 km
0.5 s
TP
LP
EP
TC
TA
RSB 9
RSB 8
Salt
Active Diapir
Fold-belt

Figure 14

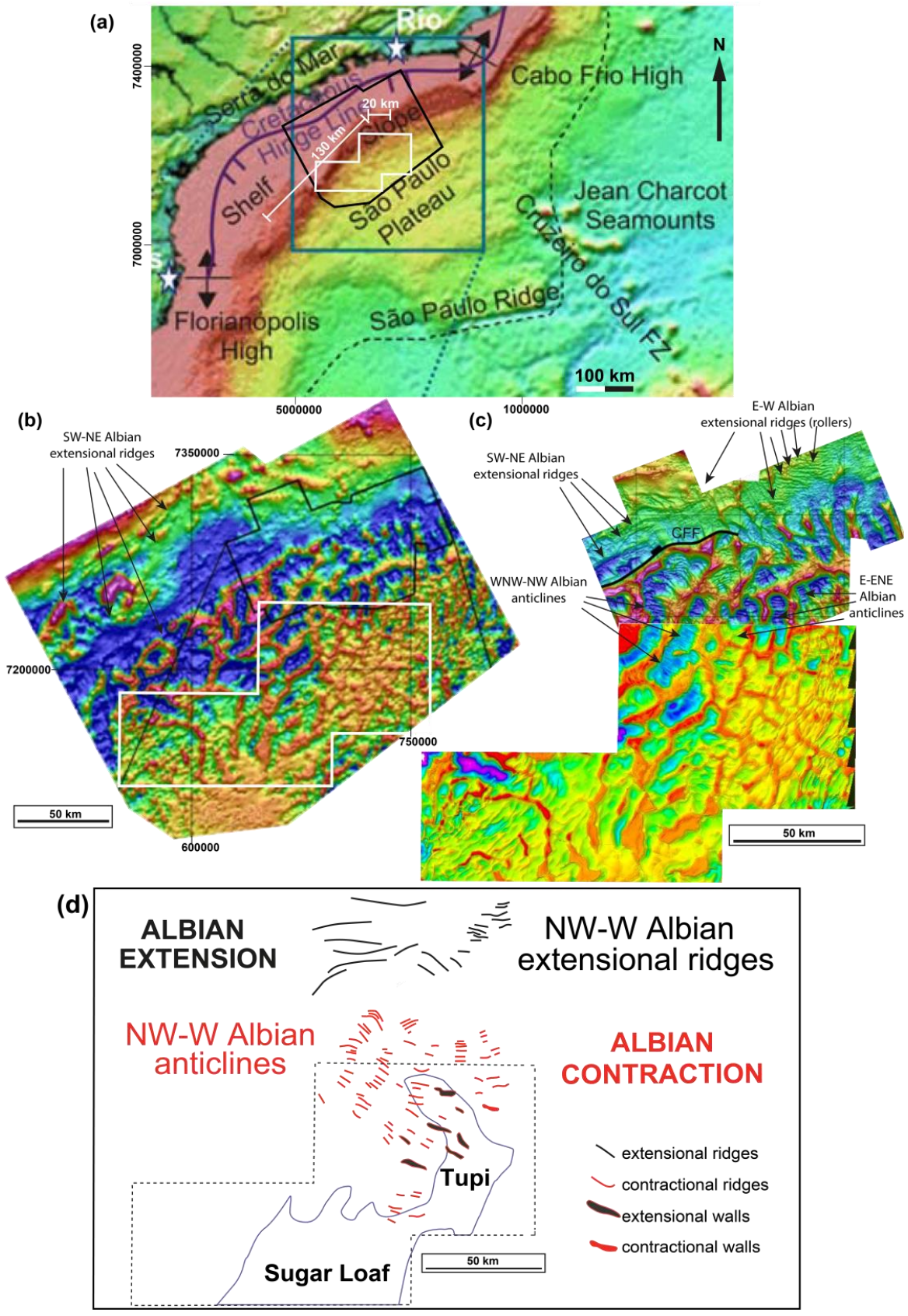
(a)
Rio
Serra do Mar
Cretaceous Hinge Line
Slope
Shelf
20 km
130 km
São Paulo Plateau
Cabo Frio High
Jean Charcot Seamounts
Cruzeiro do Sul FZ
São Paulo Ridge
Florianópolis High
100 km
N
7400000
7000000
5000000
1000000
(b)
SW-NE Albian extensional ridges
7350000
7200000
750000
600000
50 km
(c)
E-W Albian extensional ridges (rollers)
SW-NE Albian extensional ridges
CFF
WNW-NW Albian anticlines
E-ENE Albian anticlines
50 km
(d)
ALBIAN EXTENSION
NW-W Albian extensional ridges
NW-W Albian anticlines
ALBIAN CONTRACTION
Tupi
Sugar Loaf
50 km
extensional ridges
contractional ridges
extensional walls
contractional walls

Figure 15

(a) Idealized flow-profile for the SPP

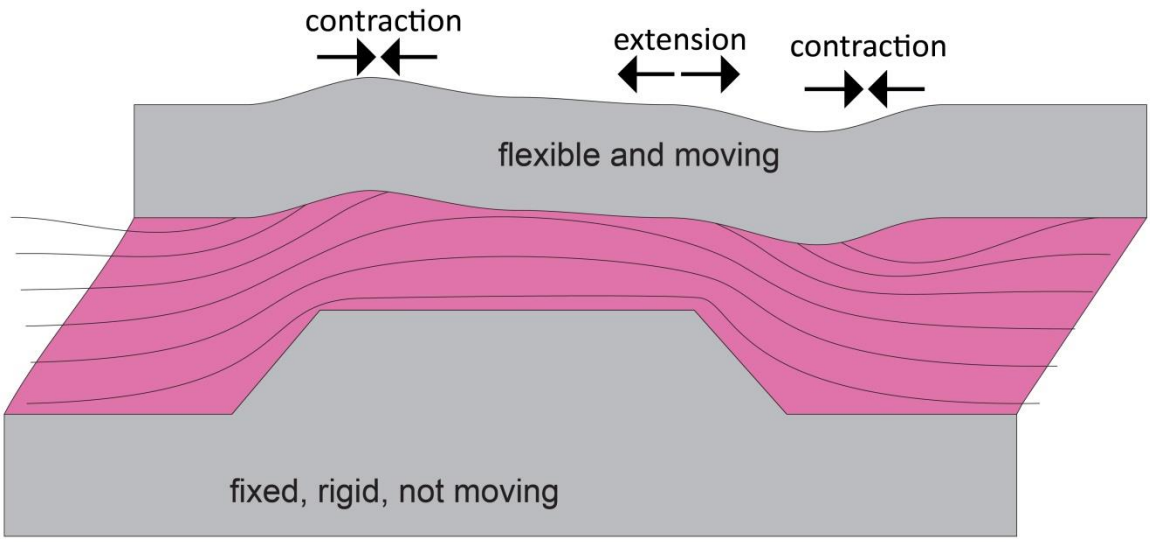

(c) Flow profile with neglible roof

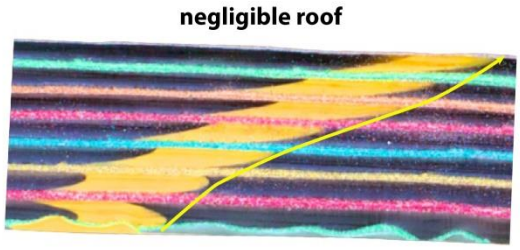

(d) Flow profile with thick roof

Figure 16

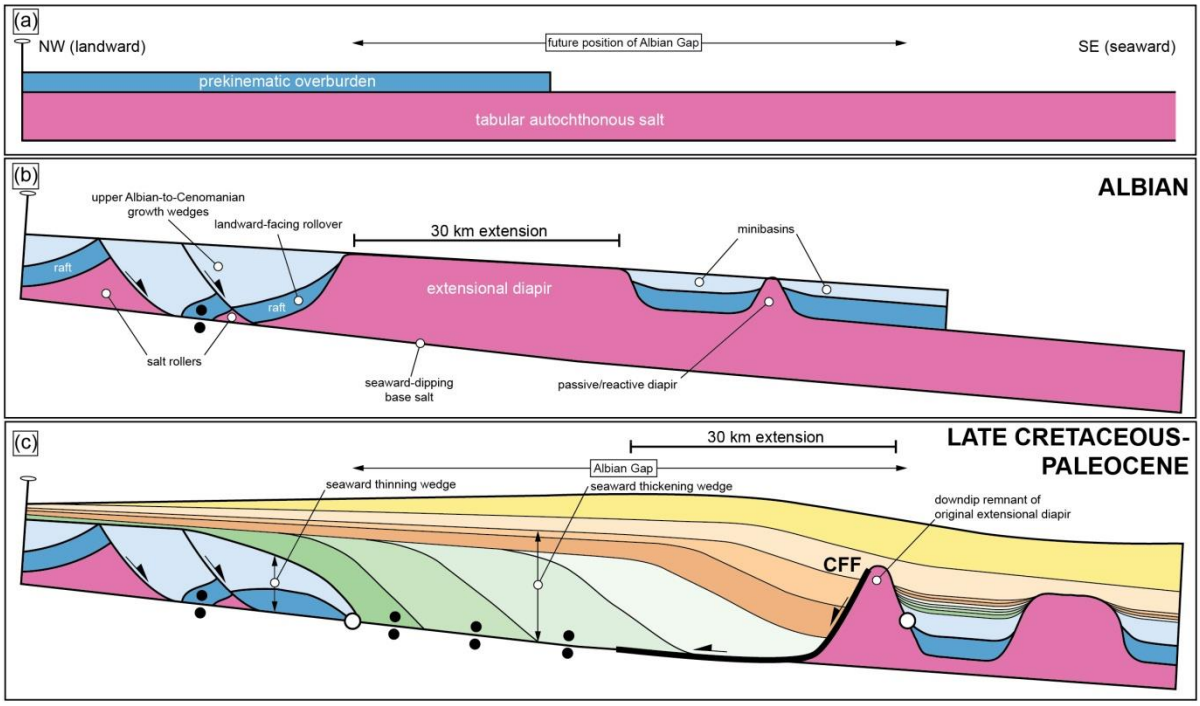
(a)
NW (landward)
future position of Albian Gap
SE (seaward)
prekinematic overburden
tabular autochthonous salt
(b)
ALBIAN
upper Albian-to-Cenomanian
growth wedges
landward-facing rollover
30 km extension
minibasins
raft
raft
extensional diapir
salt rollers
seaward-dipping
base salt
passive/reactive diapir
(c)
30 km extension
LATE CRETACEOUS-
PALEOCENE
Albian Gap
seaward thinning wedge
seaward thickening wedge
downdip remnant of
original extensional diapir
CFF

Figure 17